REVIEW

Check for updates

Single atoms supported on metal oxides for energy catalysis

Runze Li, Lei Luo, Xinlong Ma, Wenlong Wu, Menglin Wang and Jie Zeng ⓘD *

Single-atom catalysts (SACs) have attracted wide interest from researchers, as they promisingly bridge the gap between homogeneous and heterogeneous catalysts. There are various types of supports reported to anchor single metal atoms. Among them, metal oxides have received much attention because of their specific and variable properties. In this review, the unique role of typical oxide supports in anchoring isolated metal atoms and participating in catalysis is emphasized. The interactions between metal atoms and oxide supports are clarified, so as to show how to stabilize the atomic metal sites and adjust the geometric and electronic structure of single atoms reasonably. Accordingly, we highlight and summarize the progress made in the synthesis of SACs in recent years, placing special emphasis on preventing isolated metal atoms from migrating or agglomerating. In addition, the modern characterization technologies of SACs are summarized and discussed, which can provide strong evidence on the geometrical structures and electronic states of SACs. Then the applications of SACs supported on metal oxides in energy catalytic reactions are reviewed, such as CO oxidation, the water–gas shift reaction, CH_4 conversion, CO_2 hydrogenation, oxygen reduction reaction, hydrogen evolution reaction, and CO_2 reduction reaction. Finally, the existing problems and development prospects in this field are discussed.

1. Introduction

Catalysis has been greatly developed in scientific research.[1,2] A high specific surface area is very important for improving the performance of catalysts, especially their activity.[3–6] The

Hefei National Laboratory for Physical Sciences at the Microscale, Key Laboratory of Strongly-Coupled Quantum Matter Physics of Chinese Academy of Sciences, Hefei Science Center, National Synchrotron Radiation Laboratory, Department of Chemical Physics, University of Science and Technology of China, Hefei, Anhui 230026, P. R. China. E-mail: zengj@ustc.edu.cn

reactants usually interact only with the active sites on the surface, and on some occasions the inner atoms play a negligible role in the reaction.[7,8] Based on this, the proportion of active surface atoms needs to be maximized. This is especially important for high-performing noble metals because they are scarce and expensive. Zhang and co-workers studied the preparation and performance of single-atom catalysts (SACs), and on this basis, put forward the concept of "single-atom catalysis" for the first time.[9] Since then, single-atom catalysis has become a cutting-edge domain of heterogeneous catalysis.[10] SACs are a type of catalyst that consist of isolated metal atoms and

Runze Li received his B.S. degree from University of Science and Technology of China in 2021. He is currently a Ph.D. candidate at Tsinghua University under the supervision of Prof. Dingsheng Wang. His research interests are focused on the design and synthesis of novel functional single-atom catalysts and their applications in energy conversion and storage.

Lei Luo received his B.S. degree (2011) and master's degree (2013) from Harbin Institute of Technology, and obtained a PhD (2019) at Shanghai Jiao Tong University. He worked with Prof. Jie Zeng as a postdoctoral fellow at University of Science and Technology of China from 2019 to 2021 and was promoted to Research Associate in 2021. His research interests are focused on the design of catalytic reaction device and selective and efficient conversion of carbon-based small molecules.

support materials.[11] The catalytically active centers in SACs are isolated metal atoms, and sometimes adjacent atoms or surface functional groups, on the surface of the support. The catalytic performance of supported single atoms is strongly dependent on the interaction with the surface of the support.[12] SACs are conceptually different from single site heterogeneous catalysts (SSHCs). According to its definition, a SSHC can be composed of more than one atom.[13] It can be composed of atomic groups, as long as all of the groups behave identically in catalysis. SACs are equivalent to SSHCs only when all of the isolated metal atoms interact with the surface or the surface functional groups of the support in the same way. Nowadays rare-earth metals can also be used to prepare SACs.[14] SACs exhibit maximized atomic utilization efficiency and can be rationally designed for target reactions on the atomic scale. However, due to the complex and changeable nature of heterogeneous metal catalysts, it is difficult for us to understand their catalytic mechanism at the

molecular level, so as to develop industrial catalysts with perfect catalytic selectivity for desired products.[15] Furthermore, the advantages of homogeneous and heterogeneous catalysis are combined in SACs and the selectivity can be increased.[16] However, characterized by their high surface energy, isolated metal atoms can easily migrate or agglomerate into clusters, and are thus considered unstable.[17–19] To improve the stability of isolated atoms, various traditional and novel synthesis methods have been developed.[20–25] Advanced characterization techniques are important to develop SACs, as they can provide useful information for determining the geometries and electronic states of SACs.[26] Moreover, SACs have been widely used not only in the fields of thermocatalysis,[27–30] electrocatalysis,[31–37] and photocatalysis,[38] but also in the fields of batteries[39,40] and organic chemistry.[41]

As far as supported metal catalysts are concerned, the morphology and the valence state of the metal structure will change according to the support materials. The range of support materials of SACs has been extended from metal oxides[42,43] to metal nanomaterials,[44] carbon-based materials,[34,36,45–55] hexagonal boron nitride (h-BN),[56] zeolites,[19] metal–organic frameworks (MOFs),[57] covalent–organic frameworks (COFs),[58] two-dimensional materials (such as MoS_2 and MXene),[59–63] and MoC.[64,65] Among the several types of supported SACs, metal oxide supported SACs have received much attention because of the specific and variable properties observed in metal oxides, including surface pH and redox properties. The reducible oxide supports exhibit various defects, including oxygen vacancies (O_v), metal vacancies (M_v), edges, steps, and terraces, which are suggested to be suitable anchor sites.[66–72] However, as all defect sites can capture metal atoms, determining the exact anchor location is quite a challenge. On the

Wenlong Wu received his Ph.D. degree from the University of Science and Technology of China (USTC) under the supervision of Prof. Jie Zeng in 2019. Then he joined USTC and was promoted to an associate research fellow in 2021. His research interests are focused on the design and synthesis of well-defined catalysts and their applications in CO_2 conversion.

Menglin Wang received her BS degree in materials science and engineering at the USTC in 2014. She received her PhD degree with Prof. Jie Zeng in the Department of Chemical Physics at the USTC. Then she joined USTC and was promoted to an associate research fellow in 2021. Her work now focuses on the precise fabrication of surface/interface structures of catalysts.

Dr Jie Zeng is a Professor of Chemistry at the University of Science and Technology of China (USTC) and PI of the Hefei National Laboratory for Physical Sciences at the Microscale (HFNL). He studied applied chemistry at the USTC (BS, 2002) and received a PhD in condensed matter physics under the tutelage of Prof. J. G. Hou and Prof. Xiaoping Wang (2007). He worked with Prof. Younan Xia as a postdoctoral fellow at Washington University in St. Louis from 2008 to 2011 and was promoted to Research Assistant Professor in 2011. In 2012, he relocated to USTC to take the position of Professor for Chemistry in Hefei National Laboratory for Physical Sciences at the Microscale. His research interests include the selective and efficient conversion of carbon-based small molecules (such as CO, CO_2 and CH_4) to liquid fuels and high value-added chemicals from both materials and mechanistic aspects.

other hand, irreducible oxides (such as Al_2O_3) have fewer surface defects, and thus their interaction with metal species is weak. Nevertheless, the surfaces of these supports usually have abundant coordinatively unsaturated sites. For instance, there are a large number of unsaturated pentahedral Al^{3+} sites on Al_2O_3, which can stabilize noble metal Pt atoms.[73] In contrast, on oxide support surfaces, transition metal atoms can coordinate with excess oxygen ions through metal–oxo/hydroxyl group (M–O(OH)) interactions.[74,75] By inhibiting possible aggregation, spatially confining isolated metal species to the porous nanostructures of oxide supports is another method to maintain atomic dispersion.[76,77] The support not only disperses and stabilizes the metal atoms, but also interacts with the metal atoms, which often leads to charge transfer on surfaces, a change in the metal structure and the modulation of molecular adsorption, thus affecting the performance of catalysts.[23,78,79] Metal–support interactions (MSI) require very prominent charge transfer between metal species and the surfaces of the supports, leading to reversible structure change at the nanoscale. The reversible suppression of CO adsorption has been observed on Pt/TiO_2 SACs.[80] Although MSI between single Pt atoms and the $TiO_2(B)$ support does not occur after low temperature reduction, the adsorption of CO on single Pt atoms completely disappears when the reduction temperature reaches 600 °C. Subsequent re-oxidation at 300 °C restores the CO adsorption on nanoparticles (NPs) and single atoms. This proves that the stopping of the CO adsorption on single Pt atoms is reversible.

We briefly introduce several typical metal oxides as supports here. Fig. 1 shows the acidity and alkalinity of commonly used metal oxide supports. The acidity and alkalinity of metal oxides reflect their affinity to electrons and protons, respectively, thereby affecting the types of adsorbed metal groups. As electrophilic supports, acidic oxides tend to adsorb electron-rich groups such as anionic clusters, while alkaline oxides tend to adsorb electron-deficient groups.[25] Meanwhile, the valence states of adsorbed metal species might be affected by the difference in the acidity and alkalinity of oxides. Iron can coordinate with oxygen easily and is a non-noble metal and one of the most abundant elements. On account of the redox properties of iron, different pretreatment methods and reaction environments can lead to different crystalline phases of iron oxides.[81] Among these oxides, FeO_x has been the most widely used and investigated as a support for SACs.[82–88] The reconstruction of $(\sqrt{2} \times \sqrt{2})$-$R45°$ on the $Fe_3O_4(001)$ surface has been determined in previous studies of SACs dispersed on Fe_3O_4, in which the subsurface Fe vacancies induce it, featuring pockets that can contain isolated atoms.[89–91] Fe vacancies are also found in iron oxides of other crystalline phases, including Fe_2O_3.[92] In addition to vacancies in defective iron oxide, strong covalent metal–support interactions (CMSI) between the metal atoms and the non-defective iron oxide can also stabilize isolated metal atoms due to the redox properties of iron oxide.

Ceria (CeO_2) has also been investigated and applied as a support for SACs, due to its unique properties.[93] CeO_2 has a high density of vacancies.[94] In addition, CeO_2 stores oxygen via a reversible process. The local coordination environment and electron states of metal atom sites in SACs can be significantly modulated after thermal activation. Metal nanocrystalline structures on CeO_2 supports can form covalent M–O bonds and promote the dispersion of metal atoms on the atomic scale after oxidative calcination.[22,95] These properties make CeO_2 a support applicable to many catalytic reactions of small molecule conversions, such as CO oxidation, semi-hydrogenation of acetylene, and CH_4 reforming.[67,68,96,97] For instance, single Au atoms tend to occupy surface Ce vacancies, thus forming a higher loading of metal species than in an FeO_x support.[72]

Titanium dioxide (TiO_2) is one of the most representative semiconductor materials and a suitable photochemical support.[98,99] In the natural environment, rutile, anatase, and brookite are three typical crystalline phases of TiO_2, of which rutile is the most stable. In thermocatalysis, electrocatalysis and chemical sensors, charge transfer can be triggered from metal atoms to the supports. This facilitates the formation of surface oxygen vacancies and Ti^{3+} sites of TiO_2, and ultimately helps construct the active interface that results from the interaction between metal atoms and TiO_2.[66,76,80,100]

In general, the interaction between metal atoms and oxides can be weakened by the reduction of the isolated metal cations to their metallic state, which eventually results in the formation of metal clusters or NPs. However, zinc oxide (ZnO) and copper oxides (CuO and Cu_2O) are able to maintain the metallic or even negatively charged states of isolated metal atoms, which is one of their most attractive properties as supports for SACs.[101–103]

Al_2O_3 has a number of particular crystalline phases.[104] In comparison to reducible oxides, Al_2O_3 has much weaker metal–support interactions to stabilize the isolated active metal atoms, so further modification of the support is usually required. For example, mesoporous alumina exhibits more Al^{3+} defects and thus improved performance when compared with traditional bulk Al_2O_3.[73,105,106] In addition, the thermal stability of SACs can be enhanced using a $MgAl_2O_4$ spinel support during severe oxidative aging.[107,108] In addition, mixing with alkaline-earth or rare-earth metal elements can also alter the bond strength between single atoms and support oxygens.[109–111] The following sections will introduce these oxides in detail.

This review will focus on SACs supported by metal oxides. The performance of SACs is closely related to their geometrical and electronic structures. Therefore, we have chosen some typical and recent examples to explore the relationship between structure and performance and understand the interactions between the single metal atoms and metal oxide support. Firstly, the preparation methods of SACs supported by metal
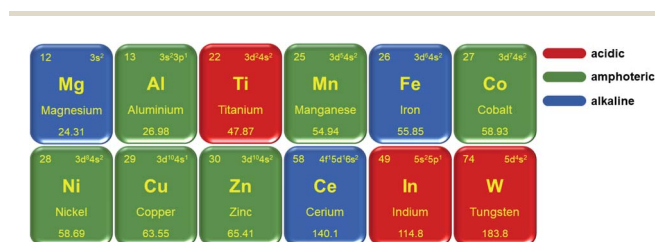

Fig. 1 Acidity and alkalinity of metal oxides.

This journal is © The Royal Society of Chemistry 2022

J. Mater. Chem. A, 2022, **10**, 5717–5742 | **5719**

oxides will be introduced, including several mature synthesis strategies. Then, based on cutting-edge characterization technologies, the importance of characterization in understanding the structure of catalysts will be emphasized, and the commonly used characterization technologies for SACs will be introduced. Finally, we will discuss the application of SACs in some important catalytic reactions, as well as the related theoretical research and reaction mechanisms. The last section gives a brief summary and prospects in the development of SACs. Some potential problems will be put forward, and the direction for the following investigations will be pointed out.

2. Preparation of SACs supported by metal oxides

The preparation of highly-dispersed single atoms on an appropriate support is a precondition for the application of SACs. Many metal oxides, including FeO_x, CeO_2, TiO_2, ZnO and Al_2O_3, are promising supports for SACs. They can not only stabilize isolated metal atoms, but also participate in reactions.[11] The surface cations of a metal oxide support can be replaced with single metal atoms and because of the interactions with neighboring oxygen anions, the metal atoms can be strongly anchored. In 2011, a co-precipitation method was employed by Zhang and co-workers to prepare Pt_1/FeO_x, which exhibits excellent activity and stability in CO oxidation.[9] Even so, preparing SACs is challenging because individual metal atoms tend to migrate and aggregate during synthesis and subsequent processing because isolated atoms usually have high surface energy, which limits the loading of isolated atoms.[112] Therefore, the improvement of metal loading at an order-of-magnitude level will bring hope to the practical applications of SACs.[113,114]

The synthetic methods generally include two categories according to the different starting metal precursors, "bottom-up" and "top-down" routes.[42,115] In the "bottom-up" route, including wet-chemistry methods, atomic layer deposition (ALD), and mass-selected soft-landing techniques, mononuclear metal precursors are deposited on the support directly or mixed with support precursor materials, while in the "top-down" strategy, metal clusters, NPs or even metal bulk are precursors. The migration of free metal precursors is limited by coordination groups (mainly hydroxyl groups) or the vacancies of oxide supports in the "bottom-up" synthesis strategy.[113] Such enhanced metal–oxide interactions are the key to stabilizing SACs. However, these SACs often suffer from low yield, low metal loading, inhomogeneous and ambiguously defined coordination environments for single metal atoms, and occasional requirements for complex or expensive equipment. On the other hand, the "top-down" strategy involves two steps, namely the breaking of metal–metal bonds in the NP precursors and the forming of a new strong bond with the surface of the support, with the potential to overcome the defects associated with the "bottom-up" strategy.[42] We will discuss some of the methods that have been widely used to synthesize SACs in this section, with emphasis on SACs supported by metal oxides.

2.1. Wet-chemistry methods

To avoid extra expense and production scale limitations, most attention has been focused on wet-chemistry methods, such as co-precipitation,[9] impregnation,[116] ion-exchange,[117] deposition–precipitation,[118] strong electrostatic adsorption (SEA),[119] *etc.*, due to their ready accessibility in most laboratories and relative ease to achieve the large-scale preparation of SACs in commercial use. The wet chemistry approach requires no special equipment and can be routinely carried out. In such a method, single metal atom species are already included in the precursor materials, and metal complexes are aimed to be anchored onto the supports without aggregation and migration during the preparation or post-treatment processes *via* a chemical reaction. As a result, strong metal–support interactions play an important role in preventing the aggregation of supported isolated atoms.

2.1.1. Co-precipitation. Different active species with uniform distribution can be obtained at the molecular scale based on the properties of co-precipitation.[11] The properties of the synthesized catalysts rely on several parameters, including the sequence and drop speed of the precursor solution, the sizes of the droplets, the efficiency of mixing, the stirring rate, the temperature of the base solution, the pH value, and the aging time.[11]

The first studied single-atom catalyst was prepared *via* a co-precipitation method.[9] Single atom Pt_1/FeO_x catalysts were synthesized in an aqueous solution of chloroplatinic acid ($H_2PtCl_6 \cdot 6H_2O$) mixed with ferric nitrate ($Fe(NO_3)_3 \cdot 9H_2O$) and sodium carbonate (Na_2CO_3) at 50 °C, and the resulting solution was controlled at a pH value of around 8. The obtained solid was dried for 5 h at 60 °C, calcined for 5 h at 400 °C and then reduced in 10% H_2/He for 0.5 h at 200 °C. A high-surface-area FeO_x nanocrystallite support with Pt metal atoms was obtained and the Pt loading was controlled to 0.17 wt%. The SACs were shown to have exceedingly high atom efficiency, distinguished stability and high activity when tested for preferential CO oxidation in a H_2-rich environment. This research shows the bright prospects for the preparation of SACs using a co-precipitation method.

A key problem in the preparation of catalysts is how to increase the metal loading of SACs. Recently, Zhang and co-workers developed their preparation method for Pt_1/FeO_x, where the Pt loading was up to 1.8 wt%, as determined by inductively-couple plasma mass spectrometry.[93] A co-precipitation method was applied in the preparation of Pt_1/FeO_x in an aqueous solution mixture of $H_2PtCl_6 \cdot 6H_2O$ and $Fe(NO_3)_3 \cdot 9H_2O$ with Na_2CO_3 solution under 3 h of stirring at 50 °C, and a further 2 h of static aging. After the filtered solids were washed with deionized water, the obtained samples were dried at 60 °C overnight. Therefore, carefully modulation of the preparation details of the co-precipitation method is vital for the preparation of SACs. The Pt_1/FeO_x catalyst exhibits excellent catalytic performance for methane combustion. In addition, many other noble metal SACs have been successfully dispersed onto FeO_x, such as Ir_1/FeO_x, the stability of which results from

5720 | *J. Mater. Chem. A*, 2022, **10**, 5717–5742

This journal is © The Royal Society of Chemistry 2022

the hydroxyl groups and the structural defects derived from the poorly crystallized FeO_x support with a large surface area.[87,88]

However, the interfacial regions of the support agglomerate or the bulk of the support crystallites can bury some metal atoms, which are major problems with this method of preparing SACs.[11] Thus, these buried single atoms cannot easily make contact with reactant molecules or may be wasted, significantly compromising the utilization of the reagents and the efficiency of the SACs.

2.1.2. Impregnation. Since all the active metal sites of prepared SACs are exposed on the surface of the supports, the use of impregnation methods can effectively prevent waste. This technology is simple: the support is immersed in a solution containing single metal precursors, and then subjected to appropriate activation treatments, such as drying, reduction, and calcination.[42] This method can be applied to almost every metal precursor and support.[116,120–126] The interaction between the metal precursors and the supports is the key in this process. The properties of the surface anchoring sites of the supports, including defects, steps, and corners determine the final loading and dispersion of the metal atoms, which prevent active metals from migrating and aggregating. Meanwhile, the metal dispersion depends on key parameters, such as the type and concentration of the metal precursors and the supports, the pH of the aqueous solution, and the surface functional groups of the supports.

Recently, Assaf and co-workers stabilized atomically-dispersed rhodium sites supported by ceria using an impregnation method.[116] A CeO_2-based support was synthesized prior to the method using cerium(III) nitrate hexahydrate solution mixed with zirconium(IV) oxynitrate hexahydrate and ammonium hydroxide. Rhodium(III) acetylacetonate was dissolved in ethanol and the CeO_2-based support was immersed in the mixture to deposit Rh on it before the solution was dried under

stirring and the obtained solid was calcined. The obtained Rh loading of Rh/CeO_2 was 0.4 wt%. Rh atoms were efficiently trapped by the doped-support, preventing their agglomeration. During CO oxidation reaction, the stability of the SAC increased within a wide temperature range (30–200 °C) because O_2 efficiently fills the vacancies in the material at low temperatures. CeO_2, as a support, can also be used to fabricate SACs based on a Pt/CeO_2 catalyst via an impregnation method for CO oxidation.[127] The synthesis method of this catalyst is shown in Fig. 2A. An isolated palladium SAC supported by ceria in the reaction of the selective hydrogenation of nitroarenes without solvent using a simple impregnation strategy has also been reported.[126] These successful examples indicate that in the fields of catalysis, CeO_2 has drawn much attention, resulting from its redox and distinct acid–base bifunctional properties. Therefore, the adsorption properties on the surface of the catalysts and the properties of the metal species are very important.

Single Ir atoms supported by titanium dioxide with a defective metastable phase (denoted as Ir_1/def-$TiO_2(B)$) was synthesized as a catalyst using an impregnation method.[121] Def-$TiO_2(B)$ with anion vacancies was obtained via the 2 h reduction of titanium dioxide with a perfect metastable phase (per-$TiO_2(B)$) under an atmosphere of 5% H_2/N_2 at 250 °C. H_2IrCl_6 solution was added dropwise under ultrasonic vibration to the dispersed def-$TiO_2(B)$ in water. After the solution was continuously stirred and the suspension liquid was centrifuged, the obtained solid was then washed and dried under vacuum. The as-obtained powder was reduced under a 5% H_2/N_2 atmosphere and the Ir_1/def-$TiO_2(B)$ catalyst were obtained. In the hydrogenation of furfural, this Ir SAC exhibits excellent catalytic performance of 99% conversion and 99% selectivity to furfuryl alcohol, as well as great stability, superior to that of Ir SACs supported by mesoporous graphitic carbon nitride, as well as Ir nanoparticles. First principles simulations reveal that the
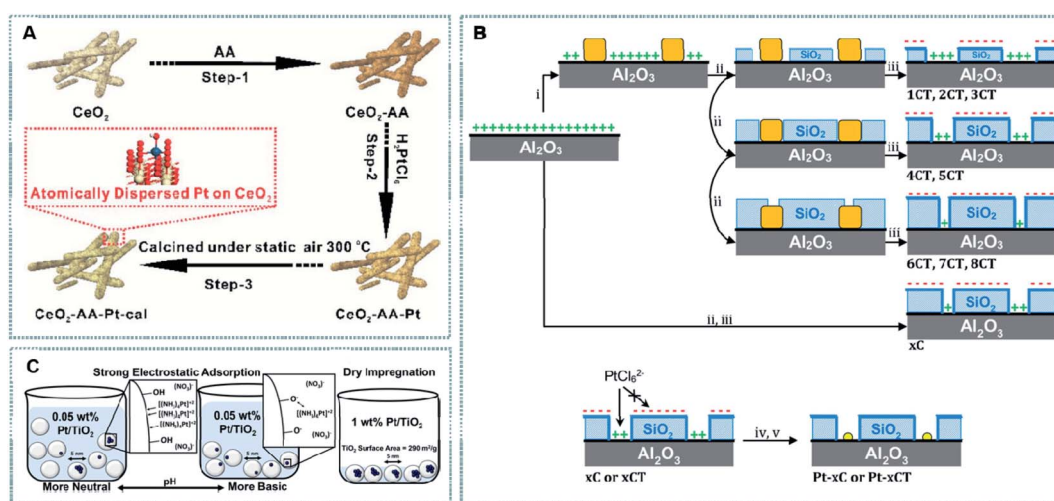

Fig. 2 (A) Schematic illustration of the L-ascorbic acid (AA)-assisted reduction synthesis of the atomically dispersed Pt/CeO_2 catalyst (CeO_2-AA-Pt-cal). Reproduced with permission.[127] Copyright 2018 American Chemical Society. (B) Support modification and Pt deposition. (i) Template grafting from toluene, (ii) x cycles of tetraethoxy orthosilicate deposition, (iii) calcination at 650 °C, (iv) SEA of $PtCl_6^{2-}$, and (v) reduction at 250 °C. Reproduced with permission.[131] Copyright 2019 AIP Publishing. (C) Synthesis approaches for producing site-isolated Pt on TiO_2. Reproduced with permission.[132] Copyright 2017 American Chemical Society.

This journal is © The Royal Society of Chemistry 2022

J. Mater. Chem. A, 2022, **10**, 5717–5742 | **5721**

regulation of the TiO$_2$ support provides appropriate interaction strength between the reactant molecules and the active metal sites, thus leading to the excellent catalytic performance of Ir$_1$/def-TiO$_2$(B). Another study utilizing the cation vacancies of supports to synthesize SACs, such as a Pt SAC with up to 2.3 wt% metal loading, was reported.[128] However, the dispersion of metal species on the support surface is often random.[42] Therefore, producing uniformly distributed SACs may be difficult.

2.1.3. Deposition–precipitation. Deposition–precipitation methods represent a step forward in producing SACs with uniform distribution at a very low metal loading.[72,129] Like the impregnation method, dispersing support precursors of metal salt or complex in solution is also required in the deposition–precipitation method, but the following procedure is different: metal hydroxides or carbonates, as metal precursors, are further precipitated on the support with metal salt complexes in the presence of a base. Modulating the pH of the solution is the key in this process. Metal precursors quickly anchor to the surface of oxides with a low metal loading, generating SACs with uniform distribution after suitable treatment.

Nanopolyhedron ceria supported atomically dispersed gold catalysts were prepared *via* a deposition–precipitation method using HAuCl$_4$ as the Au precursor.[118] A surfactant-assisted co-precipitation method was used to pre-prepare the CeO$_2$ NP support. The CeO$_2$ support was dissolved in ultrapure water and then stirred with ammonium carbonate. Under continuous stirring, HAuCl$_4$ solution was added dropwise to the above and fully mixed, and then the resulting solution was aged for 1 h. The filtered and washed solids from the suspension liquid were then subjected to 3 h of drying at 70 °C. Under the reaction conditions, the 1 wt% Au/CeO$_2$ catalysts with weakly anchored gold species exhibited high reactivity for CO oxidation, resulting from the Au$^{\delta+}$ clusters transformed from partial atomically-dispersed gold.

A deposition–precipitation method was used to synthesize iron–ruthenium oxide samples supported by ceria.[130] A hydrothermal method was first used to synthesize ceria nanorods. Under vigorous stirring, the calcined CeO$_2$ nanorods as well as (NH$_4$)$_2$CO$_3$ were dispersed in 100 mL of water. A mixed aqueous solution of Fe(NO$_3$)$_3$·9H$_2$O and RuCl$_3$·H$_2$O was added dropwise to the above solution to form a resulting solution with a pH value of ~9. The obtained greenish slurries were further aged at room temperature. Then, the washed powders were dried and calcined in air. When the secondary metal (ruthenium) was added, Fe dispersion on ceria nanorods was facilitated, and the selectivity of methane for the iron oxide catalyst supported by ceria in the Fischer–Tropsch synthesis (FTS) was improved. The change in the subnanometer iron oxide species to single atoms of ionic Fe$^{\delta+}$ was confirmed after the catalytic FTS.

Although the deposition–precipitation method is very useful when preparing uniformly distributed SACs, this method may not be useful for the high loading of metal atoms. Small metal (hydroxide) clusters or NPs may form before these metal ions are adsorbed by the supports in solution, restricting the increase in loading. This encourages us to engineer anchoring sites on surfaces, including increasing the support surface area,

fabricating more anchoring sites, and controlling the interactions between the metal and the support surfaces in solution.[129]

2.1.4. Strong electrostatic adsorption. Strong electrostatic adsorption (SEA) refers to utilizing the electrostatic interaction of the support surface to selectively deposit metal precursor ions. Strong electrostatic adsorption produces metal SACs, especially noble metal SACs, on support surfaces *via* the strong adsorption of metal complexes. Hydroxyl groups usually exist on the surface of oxides. The oxides can be positively or negatively charged when dispersed in an aqueous solution, lying on the isoelectric point (IEP) of the oxide, according to the ionic strength and pH of the solution.[131] The IEP of the oxide support can be easily modulated by coating other oxide materials on a fraction of its surface. For example, the surface hydroxyl groups can be deprotonated if the solution pH is adjusted to a point above the IEP of the oxide. Therefore, *via* coulombic forces, metal cations are strongly adsorbed on the negatively charged oxide. After the metal ion complexes are strongly anchored onto the support surfaces, the undesired ligands of the metal precursors can then be removed *via* a post-treatment process and the maximum loading of single metal atoms can be realized.

As shown in Fig. 2B, Notestein and co-workers prepared small Pt clusters, including a great portion of single Pt atoms, by combining H$_2$PtCl$_6$ SEA and oxide supports *via* engineering.[131] Controlled amounts of SiO$_2$, grafted with bulky organic templates in advance, were deposited onto Al$_2$O$_3$ to synthesize the supports (SiO$_2$@Al$_2$O$_3$). Like SiO$_2$, oxide supports with largely negative charge have small patches of Al$_2$O$_3$ with positive charge after the templates are removed, which is derived from the previously template covered regions. As the quantity of SiO$_2$ increases, Pt is deposited with a loading from 1 wt% to 0.05 wt% on templated SiO$_2$@Al$_2$O$_3$ using SEA with a pH of 4. Pt loading drops to near zero without a template. This appears to be a feasible method to generate patches of charge on oxide supports to create supported SACs with extremely high dispersion.

Isolated Pt atoms supported on TiO$_2$ was prepared as a catalyst using SEA with low loadings (0.025–0.15 wt%).[132] The TiO$_2$ support was dissolved in deionized water mixed with NH$_4$OH, resulting in a solution pH of 12.2 (Fig. 2C). Pt(NH$_3$)$_4$(NO$_3$)$_2$ solution was injected very slowly into NH$_4$OH with constant stirring to form a precursor solution at pH = 12.2. This solution was then injected into the support solution. After post-treatment, TiO$_2$ supported isolated Pt atoms were obtained. Compared to 1 nm clusters of metal Pt, isolated Pt shows a higher turnover frequency (TOF) with double the CO oxidation performance and an identical reaction mechanism at 200 °C. It was interpreted that the active site of CO oxidation on Pt supported by TiO$_2$ is interfacial cationic Pt atoms, demonstrating that isolated Pt species exhibit optimal reactivity when supported on TiO$_2$, as every atom is exposed and an interfacial site with the support is created.

It is important to point out that functional group ions usually distributes on supports heterogeneously, and the adsorption behavior of metal complexes is significantly influenced by the presence of surface defects of various types.[11]

5722 | *J. Mater. Chem. A*, 2022, **10**, 5717–5742

This journal is © The Royal Society of Chemistry 2022

Furthermore, changing the adsorption time usually leads to shifts of solution pH and consequently the quality of SACs is affected. Surfaces of the support functionalized with strong anchoring species play an important role in successfully developing stable SACs.

2.1.5. Sol–gel method. The sol–gel method is a wet-chemistry methods that is used as a general method to synthesize mesoporous oxides nanomaterials. Oxide supported SACs can be synthesized when single metal precursors are added into starting materials.[73,133] Frenkel and co-workers synthesized a Pt catalyst supported by nano CeO_2 with atomic dispersion *via* a sol–gel method.[133] The precursors, Pt-doped nanoparticles of $Ce(OH)CO_3$, were deposited on a commercial CeO_2 surface to generate single-surface Pt atoms with nearly homogeneous dispersion supported by CeO_2. The structural phase transformation of precursors was triggered by subsequent calcination and isolated Pt atoms supported on the surface of CeO_2 nanoparticles were formed. The Pt loading on the support surface was increased by the sol-based "impregnation" process. The pores of the support firmly confined single metal atoms, resulting in good stability. However, some metal active species were buried inside the oxide materials, leading to a decrease in activity.

2.2. Physical deposition methods

2.2.1. Atomic layer deposition. Atomic layer deposition (ALD) is a method of plating material onto the surface of a support layer by layer in the form of a single atomic thin film.[134] As a technique for the deposition of metals and metal oxides, ALD technology can be used to deposit particles ranging from NPs, to subnanometer clusters, to single atom structures with a high aspect ratio and uniformly distributed porous materials due to its remarkable advantages in the preparation of homogeneous, ultrathin films. In general, ALD processes include three types: thermal ALD, catalytic ALD, and plasma-enhanced ALD (PE-ALD). Similar to chemical vapor deposition (CVD), ALD depends on a series of self-limiting and molecular-level surface reactions between the vapors of precursors and the supports.[135] ALD is a cyclic "bottom-up" method by which to support catalysts with nanostructures with near atomic precision.
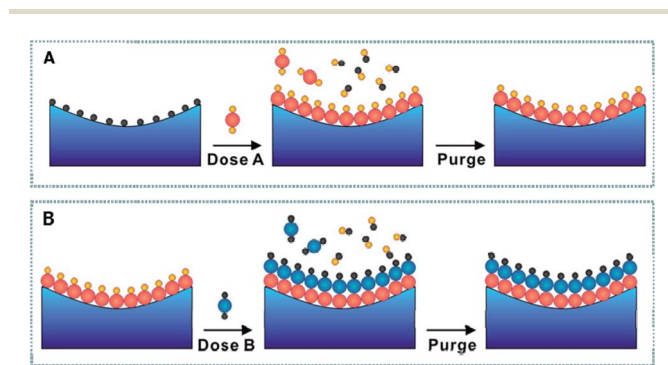

Fig. 3 (A) General ALD binary reaction sequence. (B) Reaction scheme for Fe ALD half-reactions. Reproduced with permission.[136] Copyright 2013 American Chemical Society.

The mechanism of ALD is shown in Fig. 3, which involves: (1) exposure to the first precursor, (2) purging of the reaction chamber, (3) exposure to a second reactant precursor, and (4) further purging of the reaction chamber.[136] During the first half of the reaction (step A), the first precursors react with all available active sites (defects or functional groups), and the precursors are partly removed from the supports. The reaction by-product and the residues of the first precursor are then cleaned away using inert gas. During the second half of the reaction (step B), the reactant precursors react with the precursors adsorbed in step A to obtain the target materials *via* removal the remaining ligand from the first precursors. During this reaction, the regeneration of active sites of the surfaces for sedimentary materials deposited in the subsequent cycle is very important. The by-products and residues of the second precursor are cleaned away with inert gas to complete a reaction cycle. This cycle is repeated to achieve the desired thickness or size. During ALD, the self-limiting reaction is the key characteristic, which allows us to accurately control the size and thickness of the deposited material on the atomic scale. At present, this method is widely utilized to prepare single noble metal atom, double noble metal atom and non-noble metal atom materials.[43,137,138] The first synthesis of SACs using the ALD method was achieved by Sun and co-workers.[139] They reported a synthesis method using the ALD technique for single Pt atoms supported by graphene nanosheets using $MeCpPtMe_3$ and oxygen precursors. In general, layer-by-layer growth patterns is preferred. However, deviations from ideal growth are commonly observed, including delayed nucleation in the initial film growth phase of metal oxidation or island growth.[11]

The deposition of single metal atoms on metal oxides by ALD technology has also been reported recently.[140] Liang and co-workers used ALD in a fluidized bed reactor to prepare single Fe atom catalysts supported by TiO_2 NPs using ferrocene and hydrogen as precursors. During the ALD process, they fed the chamber with $Fe(Cp)_2$ and H_2 separately *via* a distributor plate. During the ALD coating process, the reactor was also vibrated using a vibrator to improve particle fluidization quality. The following steps were involved in a typical ALD coating cycle: ferrocene dosing, N_2 purge, evacuation; H_2 dosing, N_2 purge, and evacuation. The Fe content reached 1.78 wt% and the sample was denoted as 15c-Fe/TiO_2 after 15 cycles of Fe ALD, and as the number of ALD cycles increased, the Fe loading of Fe/TiO_2 particles increased almost linearly, which indicated that Fe species deposited uniformly during every ALD cycle. In the ALD process, the dosing time of $Fe(Cp)_2$ is important in the formation of single Fe atoms. If the Fe dosing time of $Fe(Cp)_2$ was short, single atoms formed, while Fe NPs formed with an extended dosing time. In the photocatalytic degradation reaction of methylene blue (MB), 2c-Fe/TiO_2, the most active catalyst among the samples, exhibited a more than 6-fold activity enhancement compared with pure TiO_2. Also, in terms of the non-noble metal Fe, Weissenrieder and co-workers also used an ALD method to synthesize isolated Fe_1O_3 sites on the surface of a $Cu_2O(100)$ single crystal with high density using the steric hindrance of the ligands.[141] Combined with O_2 molecules, the gas phase precursor, ferrocene ($Fe(Cp)_2$) was used to achieve

This journal is © The Royal Society of Chemistry 2022

J. Mater. Chem. A, 2022, **10**, 5717–5742 | **5723**

isolated Fe$_1$O$_3$, which occupied a single site per surface unit cell, coordinating to two oxygen atoms from the Cu$_2$O lattice and another through abstraction from O$_2$. Iron densities on the surface reached 0.21 per Cu$_2$O(100) surface unit cell.

Cu single atoms supported by alumina was synthesized as a catalyst using ALD by Lu and co-workers.[20] Copper(II) hexafluoroacetylacetonate hydrate (Cu(hfac)$_2$) mixed with formalin (37% HCHO and 15% CH$_3$OH in aqueous solution) was used as a precursor and spherical alumina powder was used as the support. On the alumina powder support, one Cu ALD cycle was performed at 250 °C to obtain the Cu$_1$ SAC. Cu ALD was performed at 300 °C for 1, 3, and 5 cycles to obtain Cu NPs with different sizes of about 3.4, 7.3, and 9.3 nm, respectively. In the case of one cycle, the difference in temperature resulted in a difference between the Cu SAC and Cu NPs of 3.4 nm, possibly because formaldehyde is a strong reducing reagent at 300 °C when removing the Cu(hfac)$_2$ precursor ligands. During complete conversion, the Cu SAC exhibited a high selectivity towards ethylene, reaching 91%, with excellent stability of over at least 40 h.

As a controlled catalyst preparation method for basic research, ALD is expected to be a powerful tool to study the relationships between the structure and performance of SACs supported by metal oxides. However, these methods may not, at least in the current situation, be used on a large scale, because the equipment is expensive and the yield of the catalysts is low.[11] In the future, reducing the cost of ALD techniques will facilitate their wider application in SAC preparation.

2.2.2. Mass-selected soft-landing. Similar to ALD, mass-selected soft-landing is another physical deposition technique. This method is extremely useful for the synthesis of metal clusters with precise control over the number of atoms down to a single atom.[21,142,143] This technique can be used to prepare model catalysts excellently to carry out fundamental studies on the interactions between the metal and support and cluster size effects on the atomic scale.[139]

During the mass-selected soft-landing procedure, the metal is vaporized by a laser evaporation source with high frequency, and a mass spectrometer is used to precisely control and load metal particles of different sizes onto the surface of the support. Taking the example of dispersed single Pt clusters on MgO(100) thin films,[142] the mechanism of the mass-selected soft-landing technique was introduced. In a typical procedure, Pt clusters are produced by a laser evaporation source with high frequency, which generates high cluster currents with single positive charge. The produced metal plasma is heated by a helium pulse, and when the helium vapor experiences supersonic expansion the clusters are grown through nucleation. Subsequently, the size of the platinum clusters is selected using a quadrupole mass filter before they are deposited onto a MgO thin film.

A study of model electrodes of Pt$_n^+$ (n = 1 to 14) supported by indium tin oxide (ITO) prepared using mass-selected soft-landing technology under ultrahigh vacuum was conducted by Anderson and co-workers.[21] They used a cluster beam deposition/surface analysis instrument comprising a laser vaporization cluster source, a guided ion mass-selecting beamline, and an ultra-high vacuum (UHV) system.[144] The main UHV chamber includes the deposition end of the cluster beam lines, spectroscopy stations for X-ray and ultraviolet photoelectron spectroscopy and low-energy ion scattering, and several mass spectrometers for the study of gas surface reactivity. This catalyst can be used for ethanol electro-oxidation. Pt coverage was identical on each electrode, and only the size of the deposited Pt clusters was different. They proved that the oxidation rates of ethanol vary with the size of the clusters due to the change in the electronic structure of the reaction centers. However, the mass-selected soft-landing technique is expensive and low yielding, which limits its wide application and thus it is clearly not suitable, at least at present, for large-scale applications in industrial catalysis.[19,42,139,145]

2.3. Re-dispersion methods

2.3.1. High-temperature atom trapping methods. High-temperature atom trapping methods are "top-down" methods. A method of this type was used for preparing ceria-supported thermally-stable Pt SACs for CO oxidation.[22] When mixed with Pt/Al$_2$O$_3$ catalysts and aged, Pt was transferred to ceria. Because of the strong interactions between Pt atoms and CeO$_2$, Pt atoms were trapped, producing Pt SACs stabilized on ceria (Fig. 4A). In general, high temperatures are harmful to the performance of catalysts because of the migration and aggregation via Ostwald ripening of single atoms on catalyst supports unless the travelling atoms can be trapped. Only the most stable sites for binding can be occupied after high-temperature synthesis, yielding sinter-resistant catalysts with atomic dispersion. After the physically mixed polyhedral CeO$_2$ underwent one week of aging with Pt/La–Al$_2$O$_3$, no obvious decrease in reactivity was observed compared to that of the fresh catalyst, indicating remarkable sintering resistance. This Pt SAC was further improved via steam treatment.[95] After 10% H$_2$O flowed treatment at 750 °C, the surface lattice oxygen was activated in the vicinity of Pt^{2+} on CeO$_2$, and thus the reactivity was improved. There was no obvious decrease in activity for CO oxidation over 8 cycles and the CO conversion was maintained at 95% during testing for over 310 h at 145 °C.

Using in situ environmental transmission electron microscopy (ETEM), Li and co-workers for the first time observed atom trapping processes, as shown in Fig. 4B.[146] ZIF-8 nanocrystals were grown on Pd NPs by mixing Pd NPs and Zn(NO$_3$)$_2$ solution with 2-methylimidazole solution. ZIF-8 crystals grew around Pd NPs to form Pd NPs@ZIF-8 composites. The Pd NPs@ZIF-8 nanocomposites were then heated at 900 °C for 3 h under an inert atmosphere, after which the Pd NPs were exhausted. After the first 0.5 h of heating, the crystal Pd NPs became larger and their size distribution became uneven. After 1.5 h, the number of Pd nanoparticles decreased significantly, and the Pd nanoparticles changed from a crystallized to amorphous state. With a prolongation of the pyrolysis time (3 h), the remaining NPs were completely decomposed, and ZIF-8 was decomposed and converted into nitrogen-doped carbon. This conversion also applies to Pt and Au. Density functional theory calculations showed that the high-temperature NP-to-SA conversion was driven by the more thermodynamically stable Pd–N$_4$ structure when the moving Pd atoms are captured on the nitrogen-doped carbon defects.

5724 | J. Mater. Chem. A, 2022, **10**, 5717–5742

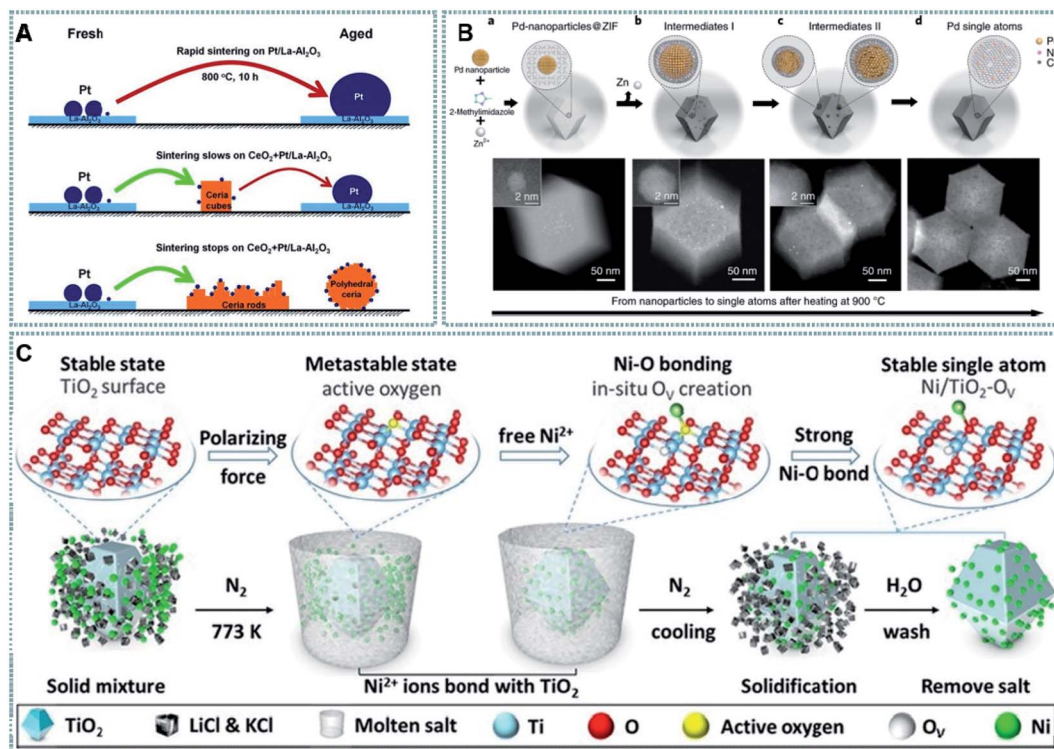This journal is © The Royal Society of Chemistry 2022

Fig. 4 (A) Illustration of Pt nanoparticle sintering, showing how ceria can trap the mobile Pt to suppress sintering. Reproduced with permission.[22] Copyright 2016 American Association for the Advancement of Science. (B) HAADF-STEM images and high-resolution HAADF-STEM images (insets) of (a) Pd-nanoparticles@ZIF-8, (b) intermediate I, (c) intermediate II and (d) Pd single atoms.[146] Copyright 2018 Springer Nature. (C) Illustration of the molten-salt-mediated preparation of atomic Ni on TiO_2, showing the TiO_2 molecular structure. Reproduced with permission.[24] Copyright 2020 Wiley-VCH Verlag GmbH & Co. KGaA, Weinheim.

2.3.2. Anti-Ostwald ripening method. The anti-Ostwald ripening method, a typical "top-down" strategy, has to date found several applications in dispersing single atoms.[23,147,148] Zhang and co-workers reported Ru SACs synthesized by physically mixing a $MgAl_{1.2}Fe_{0.8}O_4$ (MAFO) spinel with sub-micron RuO_2 aggregates.[23] A strong covalent metal–support interaction (CMSI) promotes anti-Ostwald ripening, thus leading to the dispersion process of Ru species. The presence of Fe atoms in the MAFO support weakens the Ru–Ru interactions in the RuO_2 aggregations. This strong CMSI between the FeO_x sites and RuO_2 promotes anti-Ostwald ripening of Ru/RuO_2, which enables Ru atoms to break free from static RuO_2 aggregations and spread to the surface of MAFO until being captured. This catalyst can be used for the decomposition of N_2O to generate molecules of O_2 and N_2.

2.4. Molten salt method

The molten salt method (MSM) is an ancient chemical preparation method, which has recently been adjusted to design and fabricate SACs.[24,149,150] Wang and co-workers exploited a novel MSM to obtain a TiO_2-supported Ni atom co-catalyst for the hydrogen evolution reaction (HER).[24] In the preparation method, LiCl and KCl were mixed to dissolve these precursors into a molten salt. A liquid phase formed when the temperature reached the melting point of this salts, and uniformly dispersed Ni ions were generated on the TiO_2 surface. Fig. 4C illustrates

the MSM synthesis procedure for the co-catalyst on TiO_2 with atomic Ni decoration. Furthermore, a metastable state of TiO_2 can be generated by the molten salt with strong polarizing force, and thus Ni–O bonds between oxygen ions on the TiO_2 surface and free-moving Ni^{2+} ions are formed.

2.5. Electrochemical deposition method

Recently, Zeng and co-workers used electrochemical deposition as a universal route for fabricating SACs (Fig. 5).[25] Such an
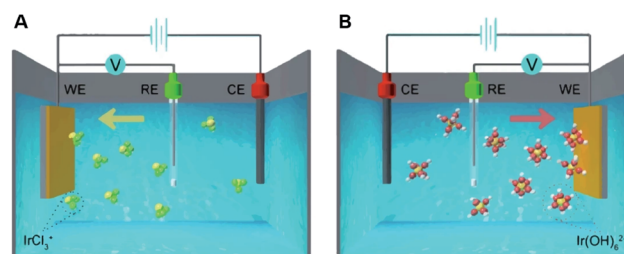

Fig. 5 Schematic of the (A) cathodic and (B) anodic deposition of Ir species, where the yellow, green, red, and white spheres represent Ir, Cl, O, and H atoms, respectively. A standard three-electrode system was used, with $Co(OH)_2$ nanosheets loaded on a glassy carbon electrode as the working electrode, a carbon rod as the counter electrode, and an Ag/AgCl electrode as the reference electrode. Reproduced with permission.[25] Copyright 2020 Springer Nature.

electrochemical deposition process is similar to the molecular mechanisms of nucleation in solution-phase synthesis, where the support can be regarded as the solvent. On this occasion, the upper mass loading limit of the SACs corresponds to the minimum supersaturation level on the support. Isolated metal atoms nucleate into clusters once the metal mass loading on the support exceeds the minimum supersaturation. Thus, controlling mass loading below the minimum supersaturation level is crucial for the formation of SACs. In addition, the minimum supersaturation level may be related to the number of deposition sites such as vacancies, edges or steps, since isolated single atoms are usually fixed to the support *via* defects or strong metal–support interactions.

2.6. Other methods

In addition, there are many other useful methods that can be adopted for preparing SACs. Metal leaching *via* a cyanide salt method has been used for synthesizing atomically-dispersed noble metals supported on oxides, such as Au/TiO_2, Au/CeO_2 and Au/Fe_2O_3, which can be applied to the water–gas shift (WGS) reaction.[151,152] A facile cation-exchange method can be used to prepare many noble metal SACs, and can even be used for large-scale production.[153,154] Iced photochemical reduction can restrict the random diffusion of mononuclear metal precursors and reduce the tendency for migration and agglomeration of metal species, leading to the generation of SACs and preventing the formation of metal NPs.[99,155]

To sum up, each method of preparing SACs has its own advantages and different applications. Wet-chemical methods are commonly used to prepare SACs and can be performed in general laboratories without special equipment. Among them, the first reported SAC was prepared *via* a co-precipitation method, but the metal atoms may be buried in the support during the synthesis process, resulting in a reduction in the utilization of the metal atoms. This problem also exists in sol–gel methods. Impregnation methods can be used to avoid this problem, since the metal atoms can be directly adsorbed on the oxide surface, but there are still issues using this method in controlling uniform dispersion. Deposition–precipitation methods can be effectively used to achieve uniform dispersion at very low loading, but it is difficult to increase the loading of metal atoms. In addition, strong electrostatic adsorption

methods also face issues in terms of uncontrollable synthesis conditions and uneven surface sites. In contrast, physical deposition methods, including ALD and mass-selective soft-landing, can achieve controlled synthesis of SACs with uniform sites, which helps us to understand their structure–performance relationship. However, these methods are often expensive and require complex equipment, and are thus not suitable for the large-scale preparation of catalysts at this stage. Moreover, many new methods for the preparation of SACs have been developed. Re-dispersion from metal nanoparticles to single atoms is an attractive method for understanding the interactions between metal atoms and supports. The preparation of SACs *via* molten salt methods is a modification of an ancient synthesis method. Electrochemical deposition is a novel general synthesis method, which has valuable application in the synthesis of precious metal SACs.

3. Characterization of SACs supported by metal oxides

Advanced characterization techniques play an important role in the development of SACs, which provide useful information on the research of the structure of SACs. The source of detection can be electrons, ions, photons, neutrons, electric field, and magnetic field (Fig. 6). In general, the structures of catalysts include both geometry and electronic structures.[55] The classical geometric structure of SACs refers to the existence of only isolated active metal atoms, which certifies the formation of single atoms directly according to definition. The electronic structure of SACs is mostly related to the electronic orbital states and the valence of metal atoms, which cannot offer direct evidence for the generation of isolated atoms, but offer deep insights into comprehending the structure–function relationship.

Directly imaging single metal atoms supported by high-surface-area materials results in the most compelling and intuitive evidence of SACs, which suggests that microscopy technologies have great applications in this field. X-ray spectroscopy can offer information about the dispersion of single atoms, the properties of the adjacent atom species, and the oxidation states of metal atoms. Infrared (IR) spectroscopy uses appropriate probe molecules to evaluate the existence and the percentage of single metal atoms on a metal oxide support to
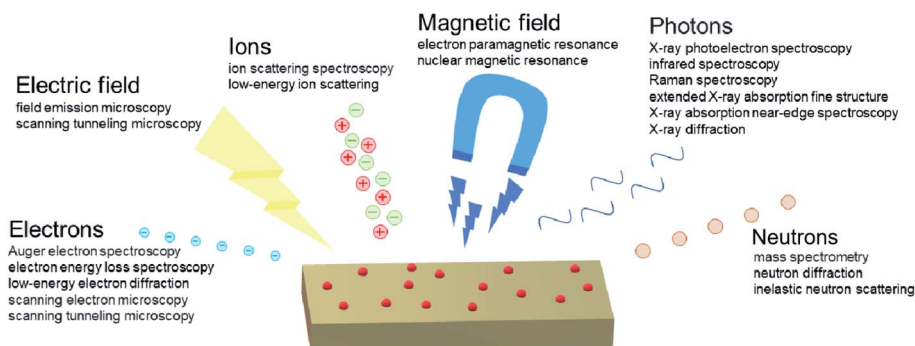

Fig. 6 Basic phenomena of characterization techniques.

5726 | *J. Mater. Chem. A*, 2022, **10**, 5717–5742

This journal is © The Royal Society of Chemistry 2022

a certain degree. In addition, electron paramagnetic resonance (EPR) spectroscopy can be used to detect unsaturated coordination species on metal oxides as well as to probe the strong interactions between single atoms and the supports. Nuclear magnetic resonance (NMR) spectroscopy offers useful information about the structure of catalysts and sorbate–sorbent interactions. *In situ* or *operando* spectroscopy can provide additional information about the properties of catalysts in their working state. Each characterization technique has its unique emphasis and advantages. Therefore, it is useful to combine multiple characterization techniques when it comes to recognizing atomically dispersed single atoms, investigating the fine structure of catalysts, and exploring the distinct performance of catalysts in various working environments.

3.1. Microscopy technologies

When it comes to reliably evaluating the quality of supported metal catalysts, especially supported noble metal catalysts, integrated electron microscopy approaches have proven to be valuable. As mentioned above, microscopy technologies can provide direct information on SACs. These methods are extremely powerful for confirming whether only single atoms exist without clusters and nanoparticles, acknowledging the single metal atom locations in relation to the support surface structure, and determining the spatial distribution of isolated atoms.[3] These techniques are indispensable for confirming that metal SACs have been successfully prepared in the process of

developing and optimizing synthesis procedures. However, the inevitable contradictions between the enlargement of the detection area and the improvement in resolution lead to the failure of microscopic techniques to reflect the overall information of the sample convincingly.

3.1.1. Scanning transmission electron microscopy. The cold-field emission electron gun was developed in scanning transmission electron microscopy (STEM) by Crewe in the early 1970s to construct a subnanometer electron probe, and the first images of electron microscopy of single uranium atoms were thus obtained.[156] STEM can provide lots of intuitive information about different materials while requiring only a small amount of sample. STEM is very useful for probing the existence of only single atoms without clusters and nanoparticles, confirming the location of supported single atoms and their spatial distribution.[9,67,72,157–159] In the past few decades, aberration-corrected high-angle annular dark-field (HAADF) imaging mode has been successfully applied to visualize single atoms (Fig. 7A and B), provide significant information about the properties of SACs supported by metal oxides and fabricate supported metal SACs using optimized synthesis methods.[160–162]

For example, isolated uniformly-dispersed Pt atoms were clearly observed from aberration-corrected HAADF-STEM images of Pt_1–Co_3O_4 catalysts.[163] STEM can also contribute towards investigating the dispersion and the spatial distribution of supported metal atoms. Zhang and co-workers observed isolated Pt atoms dispersed on Pt_1/FeO_x by aberration-corrected HAADF-STEM and a portion of the Pt atoms were found to be
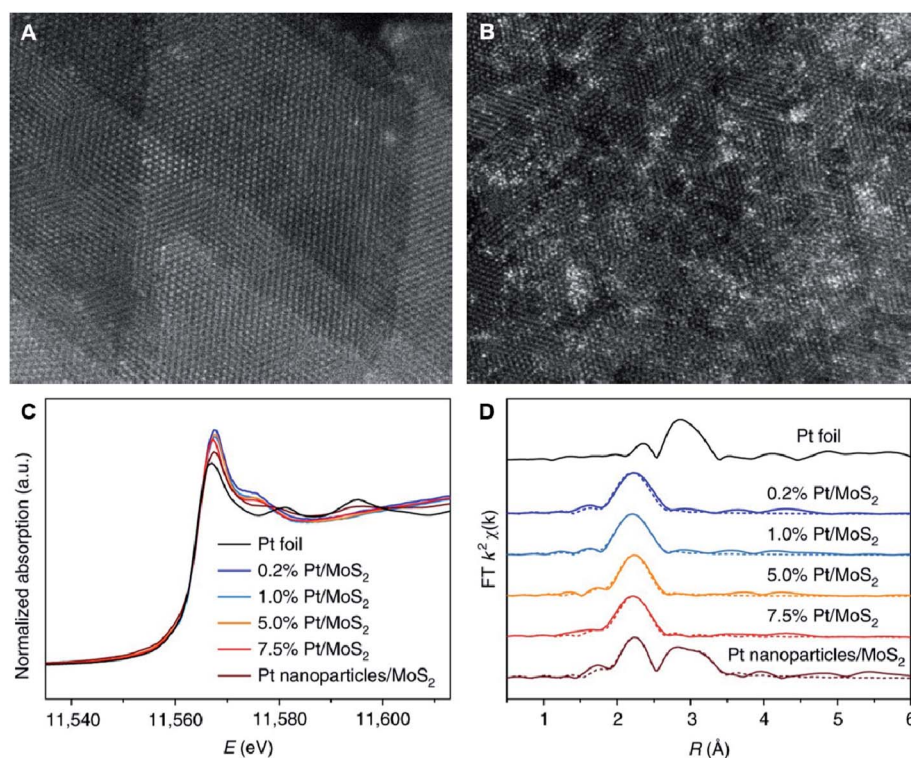

Fig. 7 HAADF-STEM images of (A) 0.2% Pt/MoS_2 and (B) 7.5% Pt/MoS_2. (C) Pt K-edge XANES spectra and (D) Pt K-edge EXAFS in *R* space for atomically-dispersed Pt/MoS_2 with different Pt loadings and Pt nanoparticles/MoS_2. Pt foil was used as a reference. The dashed lines in (D) are the corresponding fitted curves. Reproduced with permission.[162] Copyright 2018 Springer Nature.

This journal is © The Royal Society of Chemistry 2022

J. Mater. Chem. A, 2022, **10**, 5717–5742 | **5727**

perfectly aligned with the Fe atomic columns.[93] Moreover, in another study, they deduced that the Pt atoms were not distributed inside the individual FeO_x nanocrystals by varying the beam focus settings.[9] The density of 0.07 Pt atoms per nm^2 in Pt_1/FeO_x catalyst was determined by examining a series of HAADF images, which were used to approximate the actual loading of Pt (about 0.09 Pt atoms per nm^2). As a result, all of the observed single Pt atoms were confirmed to be located on the surfaces or in the adjacent subsurface of FeO_x nanocrystallites.

3.1.2. Scanning tunneling microscopy. Scanning tunneling microscopy (STM) is a technique that is complementary to STEM. High-resolution imaging is performed in an ultra-high vacuum chamber with a base pressure of less than 1×10^{-10} mbar. This technique is a helpful tool to detect the composition, structure, and electronic structures of the probed SACs in some cases.[71,164,165]

After Au was deposited on $TiO_2(110)$ with a 0.08 monolayer (ML), an STM image of the catalyst was recorded.[166] The observed smallest Au spots were assigned to Au_1 species, while the larger ones were assigned to Au_3 species. Some O_b-vacs were filled by isolated Au atoms on the r-TiO_2 after deposition.

3.2. X-ray technology

It is worth noting that among the characterization techniques, XAS and XPS provide important information on the relationship between the structure and performance of catalytic reactions, although they cannot be used to determine the formation of SACs directly.[167] However, when these techniques are applied to SACs, the results obtained by XPS are not accurate enough, but the adsorbate state splitting can reflect the strength of interactions.[55]

3.2.1. X-ray absorption spectroscopy. X-ray absorption spectroscopy (XAS) is a technique with element specificity that provides information on both geometric structure and the electronic state of molecular complexes, metal clusters and SACs.[168–170] XAS is one of the technologies used to probe the metal–support interface, which plays an important role in such catalysts with supports acting as ligands.[171] The electron donating properties and coordination geometry of isolated metal atoms affect how the reactants combine with the metal atoms, enter the catalytic cycle, and turn into the products, and how the isolated atoms resist sintering at high temperature during the reaction. Broadly speaking, there are two types of XAS: extended X-ray absorption fine structure (EXAFS) and X-ray absorption near-edge structure (XANES) spectroscopy.[172–174] EXAFS is characterized by small oscillations above the absorption edge, which can be extended to a few hundred eV, offering quantitative data on atomic spacings, coordination number and the concentration of the adsorbed atoms. On the other hand, XANES is characterized by peaks, shoulders, and other features near or on the edge of X-ray absorption spectra, offering valuable data on the oxidation states, coordination information and *in situ* results of the absorption atoms. Successful cases have been made in the field of SACs (Fig. 7C and D).[162]

As for noble metal Rh single atoms supported by CuO nanowire arrays on a copper foam (Rh SAC–CuO NAs/CF),

structural and electronic information about the Rh species was acquired from XANES and EXAFS spectra at the atomic level.[154] It was indicated that the valence of the CuO NA-supported Rh atoms is similar to that of Rh^{3+} in Rh_2O_3. As shown in the EXAFS spectra in R space, only a significant peak for Rh–O at around 1.5 Å in the Fourier-transformed (FT) k^3-weighted EXAFS spectrum can be observed, while there is no Rh–Rh peak or Rh–O–Rh peak in the spectrum of the Rh SAC–CuO NAs, indicating the presence of atomically-dispersed Rh atoms in the CuO NAs. Similarly, as revealed by the XANES at the Ir L_3-edge of Ir–NiO, the main peak is located near the same location as IrO_2, indicating an Ir oxidation state of 4+ in Ir–NiO.[175] After Ir doping, the oxidation state of the Ni atoms is slightly higher than 2+. By checking the EXAFS, it was found that the local coordination structure of Ir atoms has some similarities with that of IrO_2, but that the second and higher shell structures are different, which may result from the formation of Ir–Ni bonds instead of Ir–Ir bonds. The EXAFS fitting of the Ni K-edge also demonstrates the same Ir–Ni scattering path, identifying the single Ir atoms on NiO. Moreover, XAS has been used to analyze other single transition metal atoms supported by different metal oxides.[9,176–179]

3.2.2. X-ray photoelectron spectroscopy. X-ray photoelectron spectroscopy (XPS) owes its quantification to Einstein's explanation of the photoelectric effect in 1905. In the 1960s, Siegbahn applied the concept of differential pumping for XPS for the first time.[180] After that, Joyner and Roberts reported the construction of an XPS system at a pressure of up to 1 mbar for research on solids in 1979, which was afterwards commercialized.[181] Since then, XPS has been developed into one of the most powerful tools for studying the valence state of SACs and surface chemical composition. Chemical states and thermal stability of metal atoms with atomic dispersion can currently be studied by *in situ*- and ambient-pressure XPS.[116,135,177,182]

Huang and co-workers studied the XPS of Ir single atoms on a NiO matrix.[154] Two sets of doublets are shown in a typical IrO_2 XPS, which may largely be attributed to Ir^{4+}, located at 62.1 and 65.0 eV and 63.1 and 66.0 eV. For Ir–NiO, the Ir 4f spectral deconvolution is a bimodal of two sets of centers that can be attributed to Ir^{4+} and Ir^{3+}, at 62.3 and 65.1 eV and 61.9 and 63.8 eV, respectively. The peaks at 66.7 and 68.3 eV can be attributed to Ni 3p. Therefore, most of the Ir atoms supported by NiO are in the oxidation state of 4+, indicating the existence of highly-oxidized single Ir atoms. As revealed by the Ni $2p_{3/2}$ of NiO and Ir–NiO, after single Ir atoms are introduced, the valence state of the Ni atoms is increased. These results are consistent with XAS findings. Besides this, Shimizu and co-workers studied the role of La in a three-way catalysis process.[109] They obtained the XPS spectrum for the N 1s of $Pd/La(15)/Al_2O_3$ (Pd loading is 20 wt% and La loading is 15 wt%). Four peaks at 404, 401, 398, and 393 eV were observed in the spectrum of $Pd/La(15)/Al_2O_3$ after NO adsorption, which can be attributed to the surface-adsorbed nitrite, molecularly adsorbed NO species, atomic nitrogen, and NO species bound on the Si substrate, respectively. The presence of atomic nitrogen indicates that even at 50 °C, NO can be dissociated over $Pd/La(15)/Al_2O_3$. The metallic Pd species supported by Al_2O_3 containing La are more deficient in electrons

5728 | *J. Mater. Chem. A*, 2022, **10**, 5717–5742

This journal is © The Royal Society of Chemistry 2022

when compared with pristine Al_2O_3, which leads to a higher NO reactivity and lower CO poisoning.

3.2.3. X-ray diffraction.
X-ray diffraction (XRD) is a widely used technique to identify the structure of crystalline material with long-range order, based on Bragg's law ($2d \sin \theta = n\lambda$). It can be used for phase identification, crystal lattice parameter determination, and quantitative analysis of mixed crystal phases. X-ray sources in regular laboratories (mainly Cu Kα radiation), are good enough to determine the structure of large nanoparticles (generally bigger than 3 nm) or bulk materials by providing high diffraction signals. X-rays produced by synchrotron radiation have a high signal-to-noise ratio with very high energy and according to Bragg's law, they can produce lower angle diffraction peaks. Therefore, XRD is not suitable for the characterization of SACs without long-range order structure. However, single atomic alloy (SAA) catalysts with delicate structure of NPs or bulk materials are expected to be detected by synchrotron XRD, in spite of their particle size being less than 3 nm.[183–187]

Cu–Pd SAA catalysts for highly-efficient NO reduction were reported by Furukawa and co-workers.[188] Deposition–precipitation and/or impregnation methods were used to prepare single metal Cu and Pd and bimetallic Cu–Pd catalysts supported by γ-Al_2O_3. X-ray diffraction (XRD) analysis showed that the composition of the Cu–Pd solid-solution alloy phase in the catalysts was close to the feed metal ratio.

3.3. Infrared spectroscopy

When a beam of infrared light with a continuous wavelength (between 400 and 4000 cm^{-1}) passes through a material, some of the light can be absorbed by the material. When the vibration frequency of a chemical bond in a material molecule is the same as that of infrared light, resonance occurs, and the molecule absorbs energy and transitions from the original ground state vibrational level to a vibrational level with higher energy. The absorption of infrared light by molecules is recorded, resulting in an infrared (absorption) spectrum.[189,190] As a relatively straightforward technique, IR spectroscopy with extraordinary molecular and surface sensitivity is ubiquitous nowadays. The most remarkable characteristic of infrared spectroscopy is that it can be used to indirectly monitor the properties and changes in adsorption sites on the surface of a catalyst by tracking the changes in the vibration frequency and intensity of the probe molecules.[191] CO is the most commonly used IR probe for characterizing the surfaces of heterogeneous catalysts.[9,116,182,192–194] IR spectroscopy with CO molecules as a probe is atomically sensitive. The metal type, adsorption type (top, bridge, three- and four-fold hollow), the oxidation states, the local geometry, and the electronic environments all affect the displacement of C–O vibration frequency, suggesting the surface sensitivity of this method. Compared with the vibrational frequency of CO adsorbed on metal single atoms, that of CO adsorbed on metal clusters undergoes red-shifting due to the interactions between the CO molecules at a close distance. Time- and temperature-resolved Fourier-transform infrared (FTIR) spectroscopy can also be used to record the intermediate species of a reaction chain.[116,195–197]

For most Pt SACs, only the absence of CO adsorption on a bridge is not very convincing to confirm the existence of Pt single atoms without clusters, as the adsorption of CO on the bridge of Pt clusters is intrinsically weak. Zhang and co-workers used FTIR spectroscopy to gain information about CO adsorption behavior.[9] For the adsorption of CO on Pt/FeO$_x$, the weak band in the FTIR spectrum at 2080 cm^{-1} can be attributed to linearly adsorbed CO on $Pt^{\delta+}$, while the strong band at 2030 cm^{-1} can be attributed to linearly adsorbed CO on Pt^0, as shown in Fig. 8A and B. The bands at 1950 cm^{-1} and 1860 cm^{-1} can be ascribed to the adsorption of CO on the interface of Pt clusters and the support and the adsorption of CO on the bridge of two Pt atoms, respectively, suggesting the existence of dimers or Pt clusters, which are not observed in Pt_1/FeO$_x$. With an increase in CO pressure, the band at 2080 cm^{-1} rather than that at 2030 cm^{-1} is almost unchanged, which indicates the interactions among adsorbed CO molecules on Pt are lacking due to the presence of isolated Pt atoms.

As for Au SACs, we take ceria-supported gold catalysts as an example. *Operando* infrared spectroscopy during the course of reactivity experiments was performed to determine the intermediate species.[197] As shown in Fig. 8C and D, on the bare ceria support (blue spectra), no adsorbed CO species were observed under reaction conditions, which are detected in the region of 2154–2177 cm^{-1}. In conjunction with density functional theory (DFT) calculations, the experimental bands observed at 2160–2170 cm^{-1}, 2125–2130 cm^{-1} and 2090 cm^{-1} can be attributed to CO adsorbed on the ceria support [CO/CeO$_2$(111)], CO adsorbed onto gold species in direct contact with the CeO$_2$ support, *i.e.*, a O$_{lattice}$–Au$^+$–CO species, and CO adsorbed on top of the gold atoms of 3D Au clusters that are not in direct contact with the support, respectively. Cationic gold was confirmed to be the active site for CO oxidation reactions in the Au/CeO$_2$ catalysts. The proposed mechanism for CO oxidation at room temperature over Au/CeO$_2$ catalysts can thus be revealed by combining IR spectroscopy and DFT calculations: the oxygen vacancy created by the oxidation of CO is refilled by gas phase oxygen, while the second oxygen undergoes reaction with CO.

3.4. Nuclear magnetic resonance spectroscopy

Apart from the above characterization techniques used for characterization, nuclear magnetic resonance (NMR) spectroscopy is useful for the analysis of SACs. NMR is based on the interaction between the nuclear magnetic moment and an external electromagnetic field.[198,199] When the spin level of the nuclear magnetic moment is consistent with the frequency of the external electromagnetic field, the nucleus absorbs the energy and the energy level transitions to produce the corresponding resonance absorption, namely nuclear magnetic resonance. Atoms with nuclear magnetic moment have different chemical environments in molecules, and will undergo resonance absorption at different frequency positions. Therefore, NMR can be used to provide information on the properties of the components and the coordination environment between single atoms and supports.[73,182] Using ^{27}Al magic-angle spinning (MAS) NMR spectroscopy, it was verified that

This journal is © The Royal Society of Chemistry 2022

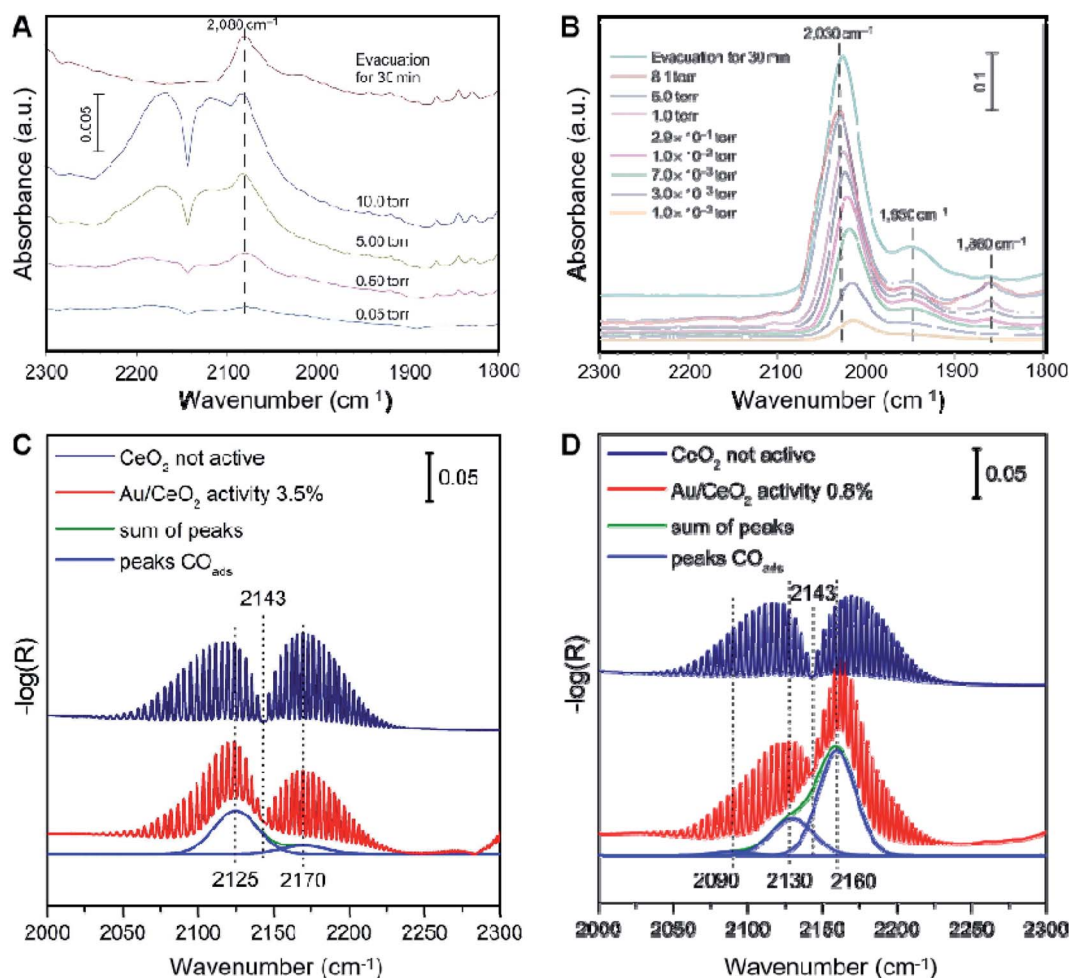*J. Mater. Chem. A*, 2022, **10**, 5717–5742 | **5729**

Fig. 8 *In situ* FTIR spectra of CO adsorption on a Pt/FeO$_x$ catalyst with Pt loadings of (A) 0.17 wt% and (B) 2.5 wt%. Reproduced with permission.[9] Copyright 2011 Springer Nature. CO stretching frequency region of *operando* infrared spectra under reaction conditions (red) after (C) equilibration in 25% O$_2$/Ar flow and (D) outgassing in 25% O$_2$/Ar at 200 °C for 1 h. Reproduced with permission.[197] Copyright 2020 Elsevier.

different preparation methods lead to different interactions between Pd atoms and Al$_2$O$_3$ supports, thus resulting in a unique electronic state of Pd species.[182] As illustrated in Fig. 9A, a considerable drop in the intensity of the peak at 35 (δ) was shown in the spectra of Pd$_1$/Al$_2$O$_3$, compared to pure Al$_2$O$_3$, which was attributed to Al$_{penta}^{3+}$ during the calcination and reduction, indicating the strong interactions between Pd atoms and Al$_{penta}^{3+}$. There was little change in the number of Al$_{penta}^{3+}$ under the same treatment in comparison with Pd/Al$_2$O$_3$, revealing weak MSI. This may result from the physical barrier of Pd precursors coated by inverse nano micelles formed in the nucleation and calcination treatment by surfactant P123.

3.5. Electron paramagnetic resonance

Since the 1960s, electron paramagnetic resonance (EPR) spectroscopy has been widely used in heterogeneous catalysis and surface chemistry for detecting paramagnetic species with unpaired electrons.[200,201] It is a powerful technique that provides information about the properties, symmetry, electronic structure, and valence state changes of paramagnetic centers and

their interactions with each other and reactants.[163,177,202,203] Song and co-workers reported TiO$_2$ NP-supported single Cr atoms with 1 wt% Cr.[202] As shown in Fig. 9B, the radicals ˙CH$_3$ and ˙OH were observed during the reaction. Titanium dioxide is known to produce surface-stable species of TiO$_2$–O$_2^-$ or Ti–OOH by activating H$_2$O$_2$, and CH$_3$OOH may be formed by the interaction of the resulting ˙CH$_3$ with Ti–OOH, which is also the main product of the original stage, as confirmed.

In addition to the characterization techniques mentioned above, there are several other techniques that can be used to confirm the geometry and electronic structure of SACs, such as Raman and UV-Raman spectroscopies, photoluminescence spectroscopy, Auger electron spectroscopy and low energy ion scattering spectroscopy, among others.[26] Furthermore, the rapidly developing *in situ* or *operando* characterization technologies can provide information on structural changes that occur under pretreatment or reaction conditions, which have become increasingly necessary and widely used to better understand the structure–property relationships of SACs. However, there is still a long way to go to realize the
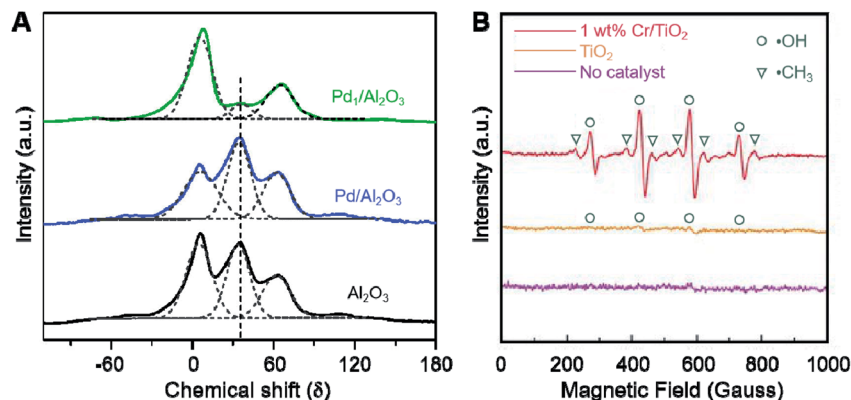
5730 | *J. Mater. Chem. A*, 2022, **10**, 5717–5742

This journal is © The Royal Society of Chemistry 2022

Fig. 9 (A) ^{27}Al MAS NMR spectra (solid lines) and their deconvolution results (dashed lines) of Pd$_1$/Al$_2$O$_3$, Pd/Al$_2$O$_3$, and Al$_2$O$_3$. Reproduced with permission.[182] Copyright 2020 Elsevier. (B) EPR experiments on oxygenated products in liquid phase with different catalysts. Reproduced with permission.[202] Copyright 2020 Wiley-VCH Verlag GmbH & Co. KGaA, Weinheim.

measurement and detection of catalysts with higher sensitivity. For example, new data analysis protocols and more powerful detectability of XAS are desired due to the limitation of supported SACs with low metal loading.[204] Further improvements on the detection limit and sensitivity of IR spectroscopy are needed for the detection of weak adsorption capability on single metal atoms and SACs with extremely low loading of metal atoms.[11]

4. Applications of SACs supported by metal oxides

SACs have been widely used in several domains of catalysis, including thermocatalysis, electrocatalysis and photocatalysis, showing special properties different from nanocatalysts due to their unique structures. In this section, we focus on the reactions catalyzed by SACs, including CO oxidation, the water–gas shift reaction, CH$_4$ conversion reaction, hydrogenation of CO$_2$, oxygen reduction reaction (ORR), hydrogen evolution reaction (HER) and CO$_2$ reduction reaction (CO$_2$RR). SACs also exhibit distinctive performances for the electrocatalytic formic acid oxidation reaction and electrocatalytic water splitting.[125,205] The mechanism of the reaction and the structure–property relationships have been investigated in detail from both experimental and theoretical aspects.
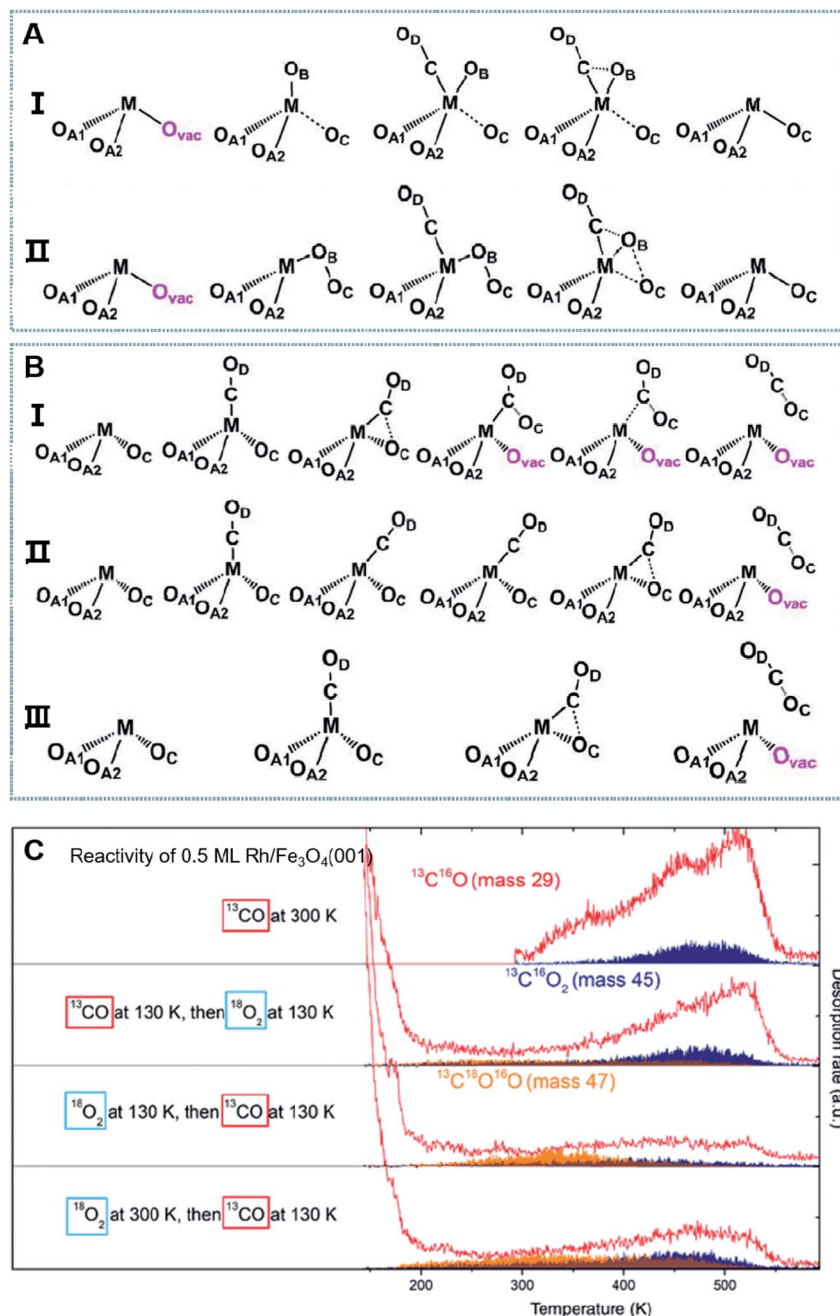
4.1. CO oxidation

As a prototype reaction, catalytic CO oxidation can be used in some industrial processes, such as the removal of CO from vehicle exhausts, the removal of CO in hydrogen and proton exchange membrane fuel cells (PEMFCs), and other examples. In particular, even a small amount of residual CO may lead to a poisoned PEMFC. Therefore, the catalyst used in the preferential oxidation (PROX) of CO must be highly selective towards CO oxidation as opposed to H$_2$ oxidation as far as possible.[27] The main challenges for CO oxidation are low activity at low temperature and poor stability at high temperature, as well as high cost due to the use of noble metals. Based on the above

considerations, research on the improvement in activity, selectivity, and stability of PROX catalysts, widening of the temperature window, and better water and CO$_2$ resistance has been carried out for decades.

Li and co-workers carried out comprehensive DFT studies to calculate the activity and catalytic mechanisms for CO oxidation by single-atom catalysts (M$_1$/FeO$_x$) with the 3d, 4d, and 5d group VIII to IB metals.[83] Noticeably, a new catalyst, Pd$_1$/FeO$_x$, was found to exhibit high activity towards CO oxidation, predicted to be even better at CO oxidation compared with Pt$_1$/FeO$_x$ and Ni$_1$/FeO$_x$ previously reported. In contrast, low activities of CO oxidation were shown in other M$_1$/FeO$_x$ SACs (M = Fe, Co, Cu; Ru, Rh, Ag; Os, Ir, Au). Moreover, it was found that the adsorption strength of CO molecules on the active sites of single atoms is the key to determining the catalytic activity of CO oxidation over SACs, since it dominates the recoverability of the surface oxygen vacancy to form a second CO$_2$ during CO oxidation. At present, there are 3 types of mechanisms for CO oxidation: Langmuir–Hinshelhood (L–H), Eley–Rideal (E–R), and Mars–van Krevelen (M–vK) mechanisms.[66,197,206,207] In realistic catalytic systems, more than one mechanism coexists. As shown in Fig. 10A, calculated results indicated that the first CO$_2$ is formed *via* the L–H mechanism with high catalytic activity in M$_1$/FeO$_x$ (M = Fe, Co, Ru, Rh, Os, Ir) *via* an oxygen dissociation mechanism and M$_1$/FeO$_x$ (M = Ni, Pd, Pt) *via* an oxygen adsorption mechanism. On the other hand, the first CO$_2$ was formed with relatively low catalytic activity in M$_1$/FeO$_x$ (M = Cu, Ag, Au) *via* oxygen adsorption mechanism. Moreover, the second CO$_2$ was formed *via* the L–H mechanism in M$_1$/FeO$_x$ (M = Fe, Co, Rh, Pd, Au) through pathway I; M$_1$/FeO$_x$ (M = Pt and Ir) through pathway II; and M$_1$/FeO$_x$ (M = Ni, Cu, Ru, Ag, Os) through pathway III (Fig. 10B).

SACs supported by FeO$_x$ are widely used for CO oxidation in experiments.[9,87,93,157,208–210] For example, CO oxidation over Au$_1$/FeO$_x$ was tested in a fixed-bed reactor using mixed gases consisting of CO (1 vol%) and O$_2$ (1 vol%) in He.[208] The 0.03Au$_1$/FeO$_x$ catalyst yielded a CO conversion of about 26% at room temperature (24 °C), about 70% at 50 °C, and 100% at 160 °C, and a 0.09Au/FeO$_x$ catalyst completely oxidized CO at

This journal is © The Royal Society of Chemistry 2022

J. Mater. Chem. A, 2022, **10**, 5717–5742 | **5731**

Fig. 10 Proposed reaction pathways of (A) the formation of the first CO_2 associated with (I) oxygen dissociation on M_1/FeO_x (M = Fe, Co; Ru, Rh; Os, Ir) catalysts and (II) oxygen absorption on M_1/FeO_x (M = Ni, Cu; Pd, Ag; Pt, Au) catalysts, and (B) the formation of the second CO_2 on (I) M_1/FeO_x (M = Fe, Co; Rh, Pd; Au) catalysts, (II) M_1/FeO_x (M = Ir, Pt) catalysts and (III) M_1/FeO_x (M = Ni, Cu; Ru, Ag; Os) catalysts, starting from the surface with the O_{vac}. Here, O_{A1} and O_{A2} represent the surface lattice O atoms of the support, the O_B and O_C atoms are derived from the dissociation of an oxygen gas molecule, and the O_D atom comes from CO gas. Reproduced with permission.[83] Copyright 2018 Tsinghua University Press and Springer-Verlag GmbH Germany. (C) Probing the reactivity of 0.5 ML $Rh/Fe_3O_4(001)$ by TPD after sequential dosing of ^{13}CO and $^{18}O_2$. The red traces correspond to ^{13}CO, the blue areas to $^{13}C^{16}O_2$ produced *via* a M–vK mechanism and the orange areas correspond to $^{13}C^{16}O^{18}O$ produced *via* a L–H mechanism. Reproduced with permission.[209] Copyright 2020 Royal Society of Chemistry.

50 °C, indicating that Au_1 supported by FeO_x nanocrystallites was more active for CO oxidation. A specific rate of 8.3 mol_{CO} g_{Au}^{-1} h^{-1} and a TOF of 0.45 s^{-1} were recorded for the $0.03Au_1/FeO_x$ catalysts, which were nearly 40 and 10 times, respectively, higher than those of 4.4 wt% Au/Fe_2O_3 catalysts. Comprehensive analyses of the used catalyst by aberration-corrected

HAADF imaging indicated that after the 100 h test, no Au nanoparticles or clusters were formed, clearly confirming the rigid structure, energetic stability, and integrity of the Au_1/FeO_x catalysts. Parkinson and co-workers studied $Rh/Fe_3O_4(001)$ model SACs for CO oxidation.[209] Superoxo species were initially bound to absorbed Rh_1 atoms resulting from the

adsorption of O_2, and Rh_1 readily agglomerated to small Rh_xO_y clusters at room temperature. However, a square-planar coordination environment preferred by absorbed Rh_1 atoms was completed by the adsorption of CO, hindering O_2 adsorption and stabilizing the Rh_1 in place. CO oxidation takes place on both oxidized Rh_xO_y clusters and carbonyl Rh_1CO, but *via* very different pathways. According to TPD measurements (Fig. 10C), when catalyzing the reaction, a Langmuir–Hinshelwood mechanism is adopted by oxidized clusters at a temperature of as low as 200 K, while a Mars–van Krevelen mechanism is adopted to form CO_2 at about 480 K by Rh carbonyls.

To overcome the low activity of CO oxidation at low temperatures, Li and co-workers developed single atom Pd/ Co_xO_y on a tunable support interface induced by a crystal facet. This SAC shows very competitive activity, with 100% conversion of CO oxidation at a low temperature of 90 °C and significant 118 h stability at 60 °C.[206] Isolated Pt atoms supported on TiO_2 nanowires can even catalyze CO oxidation at room temperature.[66] The stability at high temperatures can also be improved by depositing single Au atoms on Co_3O_4, which maintains the activity after a 10-cycle temperature-programmed reaction from -100 to 300 °C or one year of storage in air.[207] Nowadays, to avoid high costs of noble metal catalysts, non-noble metal SACs have gradually come into use for CO oxidation.[140]

4.2. Water–gas shift reaction

Water–gas shift reaction (WGS) is one of the most general reactions for energy conversion, which involves the reaction $CO + H_2O \rightarrow CO_2 + H_2$. The produced H_2-rich fuel gas can be widely used in fuel cells and other applications.[65,211,212] Traditional catalysts of Cu–Zn type have been widely used for WGS, but their stability is poor at high temperature and their activity is poor at low temperature.[42] Meanwhile, supported Pt, Au and other noble metals with atomic dispersion have been intensively investigated, and are considered as promising candidates for optimal metal–support interaction and can be further modified to improve performance.[82,213–216] However, the high cost of noble metals restricts their applications industry. Moreover, the utilization efficiency of traditional supported catalysts made of noble metals is far from satisfactory.

Ir_1/FeO_x SACs with dual metal active sites that drive the redox mechanism for WGS were reported by Zhang and co-workers.[82] The mechanism of these SACs is different from that of the formation of intermediate carboxyl or formate *via* a conventional associative mechanism.[214,217,218] Upon the dissociation of water, OH* is formed on a single Ir_1 atom, while H* is formed on the first-neighboring O atom bonded to an Fe site. CO_2 is produced by the reaction between the CO adsorbed on Ir_1 sites and another O atom adjacent to it, generating an oxygen vacancy (O_{vac}). Then, H from adsorbed OH* migrates to Ir_1 and reacts with another H* subsequently to form H_2. A new WGS pathway was confirmed *via* the interaction between Ir_1 and the sub-neighboring Fe specie, which is characterized by electron transfer from $Fe^{3+}-O\cdots Ir^{2+}-O_{vac}$ to $Fe^{2+}-O_{vac}\cdots Ir^{3+}-O$ at the active site with the participation of O_{vac}. The activity of Ir_1/FeO_x

is higher than the counterparts of its cluster and nanoparticle by 1 order of magnitude and is even higher than those of Au- or Pt-based catalysts with usual high activity.[88] At 300 °C, the $Ir_1/$ FeO_x catalyst shows a remarkable reaction rate of 43.4 mol_{co} g_{Ir}^{-1} h^{-1}, as well as a TOF of 2.31 s^{-1}.

Single noble metal (Ru, Rh, Pd, Ag, Os, Ir, Pt, and Au) atoms supported by 5 different clusters of metal oxide ions ($Al_3O_5^+$, $Ce_2O_4^+$, $V_2O_6^+$, FeO_3^-, and $Ti_3O_7^-$) were studied to explore their WGS activity using DFT calculations.[219] The results indicate that the d orbitals of the noble metals and the 2p orbitals of the *ortho* oxygen strongly hybridize, leading to an apparent charge shift of the noble metal atoms, and thus positive charge centers are formed, which are favorable for catalytic reaction. The d-band center values of Ru, Rh, Os, and Ir are generally close to the Fermi levels, so high activity can be anticipated on these metals. Among the metal oxide ions studied, $RhAl_3O_5^+$ has the step with the lowest-energy barrier, which enables it to become a most promising WGS catalyst.

4.3. CH_4 conversion reaction

The energy and environmental implications of converting methane, a greenhouse gas, into a usable chemical are self-evident. However, a typical unsolved problem in catalysis is that corrosive or expensive reaction media or oxidants are involved in this reaction, making it unsuitable for commercialization.[220] Even though molecular oxygen can be used to directly convert methane to methanol in the gas phase under mild conditions, the conversion is usually hard to use in terms of stoichiometry or low reactivity and yield. Reactions yielding methanol, formic acid, ethylene, acetylene, or acetic acid by the reactant methane are continuously being researched in SACs.[68,202,220–225] Considering the high bond energy of C–H and the highly symmetric tetrahedral structure of methane, the activation of C–H bonds is the critical step in methane upgrading reactions,[225] even though the states of the active intermediate CH_3 and the products are far from each other in different reaction systems.[68,202,222,223,225,226]

As a well-studied reaction, the dry reforming of methane (DRM) has important scientific and industrial significance.[226–228] Methane mixed with CO_2 can be converted into value-added chemicals *via* intermediate syngas consisting of H_2 and CO in equal proportions. The syngas can be used to synthesize long chain hydrocarbons and oxygenated chemicals including oxo-alcohols, dimethyl ether, and acetic acid. Furthermore, by conducting a WGS step in advance, a portion of CO can be reacted with H_2O to give H_2, and thus the H_2/CO ratio can be adjusted to 2.0 before methanol synthesis and FTS.[229–231] Hu and co-workers reported a synergistic role of isolated Ni_1 and Ru_1 sites on a CeO_2 nanorod surface, namely $Ce_{0.95}$- $Ni_{0.025}Ru_{0.025}O_2$.[226] In the reforming of CH_4 using CO_2, two sets of isolated atom sites on the surface of this catalyst exhibit a high activity at 560 °C, with 98.5% selectivity to H_2 and a production of 73.6 H_2 molecules on each site per second (Fig. 11A and B). The apparent activation barrier is lower and the turnover rate to produce H_2 and CO is higher compared with catalysts with only Ni_1 or Ru_1 sites, which evidences a synergy
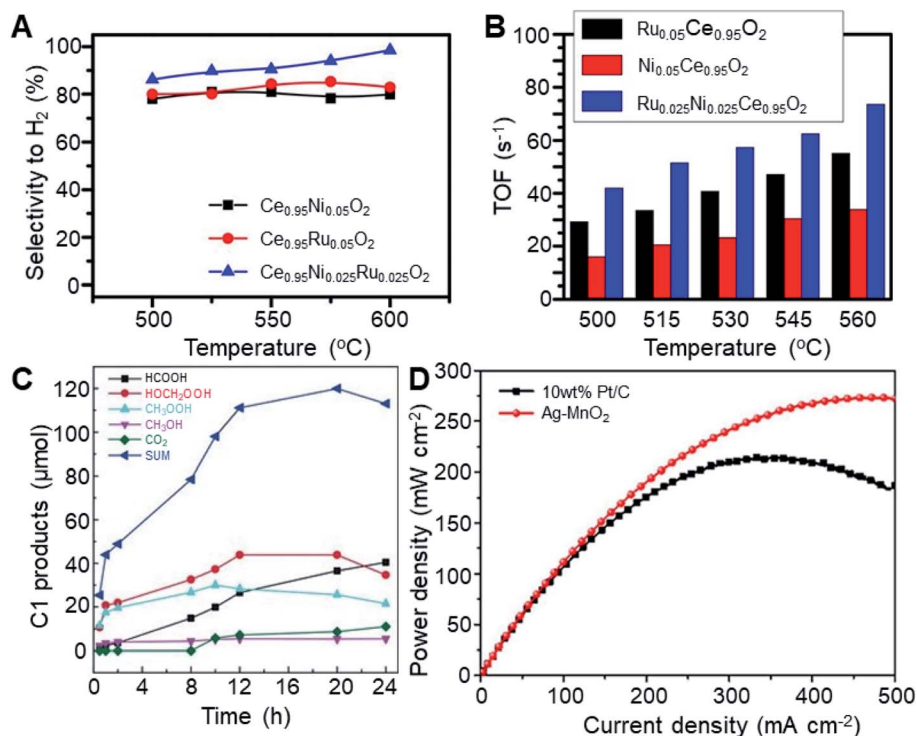
This journal is © The Royal Society of Chemistry 2022

J. Mater. Chem. A, 2022, **10**, 5717–5742 | **5733**

Fig. 11 (A) Selectivity for producing H_2 and (B) TOF of $Ce_{0.95}Ni_{0.05}O_2$, $Ce_{0.95}Ru_{0.05}O_2$, and $Ce_{0.95}Ni_{0.025}Ru_{0.025}O_2$ for the reforming of CH_4 using CO_2. Reproduced with permission.[226] Copyright 2019 American Chemical Society. (C) Catalytic performance of the 1 wt% Cr/TiO_2 catalysts for CH_4 oxidation for different reaction times. Reproduced with permission.[202] Copyright 2020 Wiley-VCH Verlag GmbH & Co. KGaA, Weinheim. (D) Power density *vs.* current density for batteries employing $Ag–MnO_2$ and Pt/C as the ORR catalysts. Reproduced with permission.[241] Copyright 2019 Elsevier.

effect. CH_4 and CO_2 are activated for the formation of CO on Ni_1 sites and Ru_1 sites, respectively. The H atoms are first generated by activated CH_4 on Ni_1 sites and then H_2 molecules are formed on Ru_1 sites by H atom coupling.

The indirect route of CH_4 conversion involves multiple steps, characterized by the addition of O atoms for the formation of syngas and the additional removal of O from CO for the formation of hydrocarbons. Therefore, direct methane conversion (DMC) to hydrocarbons is more economical and environmentally friendly without the intermediate step of going *via* syngas.[232,233] Under mild conditions, single Cr atoms supported by TiO_2 nanoparticles can be used as effective heterogeneous catalysts with H_2O_2 as an oxidant to directly oxidize methane to C_1 oxygenated products (Fig. 11C).[202] At 50 °C over 20 h, the highest yield of C_1 oxygenation product was 57.9 mol mol_{Cr}^{-1} with a high selectivity of 93%, which was remarkably higher than most relative catalysts. The mechanism of methane conversion can be interpreted as a methyl radical pathway, which first produces CH_3OH and CH_3OOH, and then $HOCH_2$-OOH and HCOOH are generated by the further oxidation of CH_3OH. The Cr atoms supported by TiO_2 activate the C–H bond of CH_4 for the formation of a $\cdot CH_3$ radical as well as H_2O_2 to form $\cdot OH$ radical. C_2 hydrocarbon product species can be also obtained *via* single atom Pt/CeO_2 catalysts for direct methane coupling without oxygen, as reported by Likozar and co-workers.[221]

4.4. Hydrogenation of CO_2

In today's world, with the consumption of non-renewable resources and the severity of environmental problems, it is crucial to reduce the dependence on fossil fuel energy and reduce carbon dioxide emissions for the sustainable development of human beings.[234]

The hydrogenation of CO_2 to turn it into liquid fuel is an effective solution.[235] Currently, many studies are devoted to catalysts for the hydrogenation of CO_2, including SACs supported by metal oxides,[193,235–240] in which an important reaction is Fischer–Tropsch synthesis. The key to the hydrogenation of CO_2 is the degree to which the carbon is coupled to the target product.

Huang and co-workers designed $Ir_1–In_2O_3$ SACs with bifunctional active centers of the single atoms and the supports for highly selective hydrogenation of CO_2 to ethanol.[235] The catalysts are efficient for the reaction in liquid, with a high selectivity of >99% for ethanol as well as an initial TOF of 481 h^{-1}. From the characterization results, it can be speculated that Lewis acid–base pairs are formed by the coupling of the isolated Ir atoms and adjacent oxygen vacancies, and thus the CO_2 is activated and intermediate carbonyl species (CO*) are formed and adsorbed on the Ir atoms. Therefore, C–C bonds can be formed when CO* species are coupled with methoxides adsorbed on In_2O_3. Pd single atoms supported by a Fe_3O_4 surface (Pd/Fe_3O_4) are also efficient catalysts for the selective hydrogenation

5734 | *J. Mater. Chem. A*, 2022, **10**, 5717–5742

This journal is © The Royal Society of Chemistry 2022

of CO_2 to ethanol.[240] These catalysts can even operate under atmospheric pressure. The special metal–oxide interface of single-atom Pd/Fe_3O_4 with a particular architecture has a favorable influence on catalytic behavior for C–C coupling.

In addition to ethanol, small molecules, such as CO and methane, can be produced by the hydrogenation of CO_2.[193,236,237] Serp and co-workers prepared Ni and Ru single atoms supported by TiO_2 with oxygen vacancies.[236] These catalysts exhibited a more active and stable performance than those atoms deposited on carbon nanotubes. By contrast, the Ni catalyst is more selective towards CO, while the Ru catalyst is more selective towards methane. For the Ru catalyst, electron-rich species orientate the selectivity towards methane, while electron-deficient species selectively produce CO, indicating a direct correlation between the hydrogenation selectivity and the electronic density of the metal.

4.5. Electrocatalysis and photocatalysis

In addition to the several applications mentioned above, SACs supported by metal oxides can also be used for electrocatalysis, such as the oxygen reduction reaction (ORR), but such reports are extremely rare. Sun and co-workers fabricated Ag atoms supported by MnO_2 nanowires with atomic dispersion (Ag–MnO_2), which can be used as an efficient cathode catalyst in rechargeable Zn–air batteries.[241] As shown in Fig. 11D, an outstanding performance was observed in a Ag–MnO_2-based Zn–air battery, exhibiting 273.2 mW cm^{-2} discharge peak power and 915.4 W h kg^{-1} energy density along with superior cycling stability, which can be attributed to the doped single Ag atoms. Atom utilization of Ag atoms in Ag–MnO_2 can be maximized and abundant oxygen vacancies are induced by Ag doping, which is beneficial to carrying out the ORR with fast kinetics. As a result of the interaction of Ag and MnO_2, the electronic structure of the active sites is rearranged after the Ag doping, thus improving the ORR activity of the Zn–air battery. In addition, single Pd atoms supported by a composite of MnO_2 nanowires and carbon nanotubes (Pd/MnO_2–CNTs) were prepared, which were applied as cathode catalysts with high efficiency in a Zn–air battery because of the synergetic effect among the Pd, MnO_2, and CNTs.[242] Superior charge–discharge ability was observed for the stable Zn–air liquid battery, with 190.7 mA cm^{-2} current density and 297.7 mW cm^{-2} peak power.

The electrocatalytic reduction of CO_2 has the potential to reduce environmental pollution and provide fuel energy by producing value-added chemicals, including alcohols and hydrocarbons, and the precise modulation of electrocatalysts on the atomic scale has achieved some improvement.[68] Multiple oxygen vacancy-bound CeO_2 with substitution by single atomic Cu was designed at the atomic level by Zheng and co-workers to electrocatalytically reduce CO_2 into CH_4, exhibiting an improved faradaic efficiency of 58%.[69] Up to three oxygen vacancies can be stably enriched around each Cu site by the single Cu atoms supported on the surface of $CeO_2(110)$, producing a catalytic center with a high efficiency for CO_2 adsorption and activation.

Lee and co-workers prepared Pt SACs supported by antimony-doped stannic oxide (Pt_1/ATO) with a Pt loading of up to 8 wt% via a conventional incipient wetness impregnation technique.[125] DFT calculations showed that it is energetically advantageous to replace Sb sites with Pt atoms in the bulk phase or at the surface of SbSn or ATO. Compared with industrial Pt/C catalysts, Pt_1/ATO showed superior activity and durability in the formic acid oxidation reaction (FAOR). In CV measurements for 1800 cycles in the range of 0.05–1.4 V, Pt retained its single-atom structure and Pt_1/ATO maintained high FAOR activity, even after rigorous durability tests. A full-cell direct formic acid fuel cell was prepared using Pt_1/ATO as the anode catalyst, and the power of the cell was found to be one order of magnitude higher than that of Pt/C.

In the field of photocatalysis, SACs can provide an opportunity to precisely control the valence state of active sites and the coordination environment on the atomic scale, showing improved performance in many model reactions. Photocatalytic reduction of CO_2 over SACs has also been reported recently.[178,243] In addition to the CO_2 reduction reaction, photocatalysis based on SACs has also made some achievements in other reactions.[24,98,140,244] For example, Wang and co-workers designed a novel molten salt method (MSM) to prepare a TiO_2-supported single Ni co catalyst for the hydrogen evolution reaction (HER).[24] In the MSM process, it is found that Ni atoms on TiO_2 are beneficial to the formation of oxygen vacancies, which facilitate the transfer of charge and the reaction of hydrogen evolution. Compared with a Ni co-catalyst on TiO_2 synthesized via an impregnation method, the synergistic effect between the atomic Ni co-catalyst and oxygen vacancies four-fold increases the H_2 evolution rate. Wang and co-workers used TiO_2 nanorod arrays for anchoring atomic-scale Bi.[98] Bi atoms with gradient distribution were assembled on TiO_2 nanorods via a one-pot hydrothermal approach. It was pointed out that the Bi ratio relatively increased as Ti species were gradually consumed in the precursor solution, resulting in a bottom-up gradient-distributed structure. An efficient charge separation and transportation channel can be realized by such a structure, and thus the HER performance can be enhanced.

5. Conclusions and outlook

Proper synthesis methods are a prerequisite for the development of catalytic science and actual practice of SACs. In this paper, the progress of synthesis methods in recent years is reviewed and classified. Methods for preparing oxide-supported SACs are commonly classified into two categories: "bottom-up" and "top-down". ALD and mass-selective soft-landing are two physical methods, which have high equipment costs. Wet-chemical synthesis includes several preparation methods, such as co-precipitation, impregnation, deposition–precipitation, strong electrostatic adsorption, and sol–gel methods, among others. In order to successfully prepare SACs, appropriate precursors of mononuclear metal complexes need to be carefully selected on the basis of the characteristics of the support, thus realizing the atomic dispersion and separation of the precursors, and inhibiting the atoms on the support from

This journal is © The Royal Society of Chemistry 2022

J. Mater. Chem. A, 2022, **10**, 5717–5742 | **5735**

migrating and aggregating. Single metal atoms on the support are stabilized by enhancing metal–support interactions.

The development of advanced characterization techniques can bring about better comprehension of structure–property relationships. HAADF-STEM and EXAFS play an important role in the characterization of the geometry of oxide-supported SACs, while XANES, XPS and EPR can be used to characterize the electronic structures of SACs. XRD is used to characterize SAA catalysts. IR spectra using CO as a probe is a powerful method to detect the local geometry, as well as the electronic environment. As stated in this article, many other characterization technologies can also be used to detect the structure of SACs.

Through the discussion of specific examples, we emphasized the potential applications of SACs for various reactions. At present, many important catalytic reactions depend on noble metal catalysts. Improving atom utilization is an effective approach to reduce the consumption of noble metals, which is of great importance to reduce catalyst costs and promote sustainability. As a widely used catalyst design strategy, oxide-supported SACs have been used for a variety of reactions for heterogeneous catalysis, including CO oxidation, the water–gas shift reaction, semi-hydrogenation reaction, CH_4 conversion reaction, oxygen reduction reaction, hydrogen evolution reaction and CO_2 reduction reaction. Fully exposed active sites, enhanced metal–support interactions, and unique electronic structures give SACs enhanced catalytic performance. In addition, due to the homogeneity and simplicity of SAC structures, this is conducive to the accurate structural recognition of the active site, which provides great potential for studying mechanisms at the atomic level *via* the combination of experiment and theory, and has important guiding significance for the rational design of catalysts.

Nowadays, the research on SACs is still in rapid development. In order to meet the needs of basic research and practical application of catalysts, increasing the loading of metal atoms in SACs and realizing the simple synthesis of SACs on a large scale are two crucial challenges in synthesizing SACs. In addition, how to effectively control the coordination environment of atoms supported by oxides has great significance, which provides broad prospects to optimize and improve the catalytic performance of SACs. The surfaces of oxides are generally not uniform, with the presence of multiple defects such as vacancies, edges, terraces, or grain/twin boundaries. Even on the same surface, *fcc* hollow sites of oxygen, *hcp* hollow sites of oxygen, and oxygen vacancy sites, among others, can be observed. These single atoms anchored on different surface sites lead to distinct electronic structures and coordination environments, which have a great influence on their catalytic properties. However, research into the correlations between the anchoring sites of single atoms on oxides and their catalytic performance are still lacking. It remains a grand challenge to precisely anchor single atoms on the specific sites of oxides. Moreover, the structure–property relationships between structure and performance and the catalytic mechanisms on the atomic scale still need to be further explored. The combination of theoretical calculations and *in situ* characterization

techniques is expected to provide valuable insights towards enhancing catalytic performance and improving the structural stability of new SACs through rational selection and design. Furthermore, the stability of SACs plays an important role in evaluating the performance of catalysts. Even though existing preparation methods can ensure atomic distribution of metal species, SACs still face the risk of loss, aggregation, or reconstruction of active sites during catalysis, especially when the high temperature and reductive atmosphere in industrial catalysis challenge their stability. Therefore, more ingenious synthesis strategies are needed to construct SACs with long-term thermodynamic stability. Moreover, we should also balance the stability and activity of the catalyst, since saturating the metal atom coordination can indeed improve the stability of the catalyst, but inevitably result in a loss of intrinsic activity. What is more, more than one atom may be involved in some reactions or elementary steps, wherein the behavior of SACs remains elusive. Double atom catalysts (DACs) with a small active unit of bridge sites, triple atom catalysts (TACs) with a small unit of hollow sites and other atomic metal catalysts are expected to solve this problem.

Conflicts of interest

The authors declare no conflict of interest.

Acknowledgements

References

1 Y. Zhao, W. Gao, S. Li, G. R. Williams, A. H. Mahadi and D. Ma, *Joule*, 2019, **3**, 920–937.
2 H. Abe, J. Liu and K. Ariga, *Mater. Today*, 2016, **19**, 12–18.
3 J. Liu, *ChemCatChem*, 2011, **3**, 934–948.
4 R. Schlogl and S. B. Abd Hamid, *Angew. Chem., Int. Ed.*, 2004, **43**, 1628–1637.
5 Y. Xia, Y. Xiong, B. Lim and S. E. Skrabalak, *Angew. Chem., Int. Ed.*, 2009, **48**, 60–103.
6 A. T. Bell, *Science*, 2003, **299**, 1688–1691.
7 H. S. Taylor, *Proc. R. Soc., Ser. A*, 1925, **108**, 105–111.
8 H. Li, L. Li and Y. Li, *Nanotechnol. Rev.*, 2013, **2**, 515–528.
9 B. T. Qiao, A. Q. Wang, X. F. Yang, L. F. Allard, Z. Jiang, Y. T. Cui, J. Y. Liu, J. Li and T. Zhang, *Nat. Chem.*, 2011, **3**, 634–641.
10 H. Ou, D. Wang and Y. Li, *Nano Sel.*, 2021, **2**, 492–511.
11 J. Liu, *ACS Catal.*, 2017, **7**, 34–59.

5736 | *J. Mater. Chem. A*, 2022, **10**, 5717–5742

This journal is © The Royal Society of Chemistry 2022

12 J. Yang, W. Li, D. Wang and Y. Li, *Small Struct.*, 2020, **2**, 2000051.

13 J. M. Thomas, R. Raja and D. W. Lewis, *Angew. Chem., Int. Ed.*, 2005, **44**, 6456–6482.

14 S. Ji, Y. Qu, T. Wang, Y. Chen, G. Wang, X. Li, J. Dong, Q. Chen, W. Zhang, Z. Zhang, S. Liang, R. Yu, Y. Wang, D. Wang and Y. Li, *Angew. Chem., Int. Ed.*, 2020, **59**, 10651–10657.

15 K. Liu, R. Qin and N. Zheng, *J. Am. Chem. Soc.*, 2021, **143**, 4483–4499.

16 J. Li, W. Wang, W. Chen, Q. Gong, J. Luo, R. Lin, H. Xin, H. Zhang, D. Wang, Q. Peng, W. Zhu, C. Chen and Y. Li, *Nano Res.*, 2018, **11**, 4774–4785.

17 Y. Zhou, X. Tao, G. Chen, R. Lu, D. Wang, M.-X. Chen, E. Jin, J. Yang, H.-W. Liang, Y. Zhao, X. Feng, A. Narita and K. Mullen, *Nat. Commun.*, 2020, **11**, 5892.

18 H. Jeong, S. Shin and H. Lee, *ACS Nano*, 2020, **14**, 14355–14374.

19 S. Ji, Y. Chen, X. Wang, Z. Zhang, D. Wang and Y. Li, *Chem. Rev.*, 2020, **120**, 11900–11955.

20 X. Shi, Y. Lin, L. Huang, Z. Sun, Y. Yang, X. Zhou, E. Vovk, X. Liu, X. Huang, M. Sun, S. Wei and J. Lu, *ACS Catal.*, 2020, **10**, 3495–3504.

21 A. von Weber, E. T. Baxter, S. Proch, M. D. Kane, M. Rosenfelder, H. S. White and S. L. Anderson, *Phys. Chem. Chem. Phys.*, 2015, **17**, 17601–17610.

22 J. Jones, H. F. Xiong, A. T. Delariva, E. J. Peterson, H. Pham, S. R. Challa, G. S. Qi, S. Oh, M. H. Wiebenga, X. I. P. Hernandez, Y. Wang and A. K. Datye, *Science*, 2016, **353**, 150–154.

23 K. Liu, X. Zhao, G. Ren, T. Yang, Y. Ren, A. F. Lee, Y. Su, X. Pan, J. Zhang, Z. Chen, J. Yang, X. Liu, T. Zhou, W. Xi, J. Luo, C. Zeng, H. Matsumoto, W. Liu, Q. Jiang, K. Wilson, A. Wang, B. Qiao, W. Li and T. Zhang, *Nat. Commun.*, 2020, **11**, 1263.

24 M. Xiao, L. Zhang, B. Luo, M. Lyu, Z. Wang, H. Huang, S. Wang, A. Du and L. Wang, *Angew. Chem., Int. Ed.*, 2020, **59**, 7230–7234.

25 Z. Zhang, C. Feng, C. Liu, M. Zuo, L. Qin, X. Yan, Y. Xing, H. Li, R. Si, S. Zhou and J. Zeng, *Nat. Commun.*, 2020, **11**, 1215.

26 M. Che and J. C. Védrine, *Characterization of Solid Materials and Heterogeneous Catalysts*, 2012.

27 H. Zhang, S. Fang and Y. H. Hu, *Catal. Rev.: Sci. Eng.*, 2020, 1–40.

28 F. Doherty, H. Wang, M. Yang and B. R. Goldsmith, *Catal. Sci. Technol.*, 2020, **10**, 5772–5791.

29 S. Kim, S. Jee, K. M. Choi and D.-S. Shin, *Nano Res.*, 2020, **14**, 486–492.

30 H. Li, M. Wang, L. Luo and J. Zeng, *Adv. Sci.*, 2019, **6**, 1801471.

31 J. Yang, W. Li, D. Wang and Y. Li, *Adv. Mater.*, 2020, **32**, 2003300.

32 T. N. Nguyen, M. Salehi, L. Quyet Van, A. Seifitokaldani and D. Cao Thang, *ACS Catal.*, 2020, **10**, 10068–10095.

33 S. Li, J. Liu, Z. Yin, P. Ren, L. Lin, Y. Gong, C. Yang, X. Zheng, R. Cao, S. Yao, Y. Deng, X. Liu, L. Gu, W. Zhou, J. Zhu, X. Wen, B. Xu and D. Ma, *ACS Catal.*, 2020, **10**, 907–913.

34 M. Huang, X. Kong, C. Wang, Z. Geng, J. Zeng and J. Bao, *ChemNanoMat*, 2021, **7**, 2–6.

35 Y. Wang, H. Su, Y. He, L. Li, S. Zhu, H. Shen, P. Xie, X. Fu, G. Zhou, C. Feng, D. Zhao, F. Xiao, X. Zhu, Y. Zeng, M. Shao, S. Chen, G. Wu, J. Zeng and C. Wang, *Chem. Rev.*, 2020, **120**, 12217–12314.

36 H. Chen, X. Guo, X. Kong, Y. Xing, Y. Liu, B. Yu, Q.-X. Li, Z. Geng, R. Si and J. Zeng, *Green Chem.*, 2020, **22**, 7529–7536.

37 L. Wang, H. Li, W. Zhang, X. Zhao, J. Qiu, A. Li, X. Zheng, Z. Hu, R. Si and J. Zeng, *Angew. Chem., Int. Ed.*, 2017, **56**, 4712–4718.

38 L. Zeng and C. Xue, *Nano Res.*, 2020, **14**, 934–944.

39 L. Peng, L. Shang, T. Zhang and G. I. N. Waterhouse, *Adv. Energy Mater.*, 2020, **10**, 2003018.

40 Z. Zhuang, Q. Kang, D. Wang and Y. Li, *Nano Res.*, 2020, **13**, 1856–1866.

41 H. Yan, C. Su, J. He and W. Chen, *J. Mater. Chem. A*, 2018, **6**, 8793–8814.

42 R. Lang, X. Du, Y. Huang, X. Jiang, Q. Zhang, Y. Guo, K. Liu, B. Qiao, A. Wang and T. Zhang, *Chem. Rev.*, 2020, **120**, 11986–12043.

43 Y. Xu, W. Zheng, X. Liu, L. Zhang, L. Zheng, C. Yang, N. Pinna and J. Zhang, *Mater. Horiz.*, 2020, **7**, 1519–1527.

44 Y. Peng, Z. Geng, S. Zhao, L. Wang, H. Li, X. Wang, X. Zheng, J. Zhu, Z. Li, R. Si and J. Zeng, *Nano Lett.*, 2018, **18**, 3785–3791.

45 E. Luo, C. Wang, Y. Li, X. Wang, L. Gong, T. Zhao, Z. Jin, J. Ge, C. Liu and W. Xing, *Nano Res.*, 2020, **13**, 2420–2426.

46 X. Yang, Y. Chen, L. Qin, X. Wu, Y. Wu, T. Yan, Z. Geng and J. Zeng, *ChemSusChem*, 2020, **13**, 6307–6311.

47 Y. Zhong, X. Kong, Z. Geng, J. Zeng, X. Luo and L. Zhang, *ChemPhysChem*, 2020, **21**, 2051–2055.

48 P.-H. Li, M. Yang, Y.-X. Li, Z.-Y. Song, J.-H. Liu, C.-H. Lin, J. Zeng and X.-J. Huang, *Anal. Chem.*, 2020, **92**, 6128–6135.

49 S. Chen, N. Zhang, C. W. N. Villarrubia, X. Huang, L. Xie, X. Wang, X. Kong, H. Xu, G. Wu, J. Zeng and H.-L. Wang, *Nano Energy*, 2019, **66**, 104164.

50 T. Zheng, K. Jiang, N. Ta, Y. Hu, J. Zeng, J. Liu and H. Wang, *Joule*, 2019, **3**, 265–278.

51 Z. Geng, Y. Liu, X. Kong, P. Li, K. Li, Z. Liu, J. Du, M. Shu, R. Si and J. Zeng, *Adv. Mater.*, 2018, **30**, 1803498.

52 J. Liu, M. Jiao, L. Lu, H. M. Barkholtz, Y. Li, Y. Wang, L. Jiang, Z. Wu, D.-J. Liu, L. Zhuang, C. Ma, J. Zeng, B. Zhang, D. Su, P. Song, W. Xing, W. Xu, Y. Wang, Z. Jiang and G. Sun, *Nat. Commun.*, 2017, **8**, 15938.

53 X. He, Q. He, Y. Deng, M. Peng, H. Chen, Y. Zhang, S. Yao, M. Zhang, D. Xiao, D. Ma, B. Ge and H. Ji, *Nat. Commun.*, 2019, **10**, 3663.

54 M. S. Kim, J. Lee, H. S. Kim, A. Cho, K. H. Shim, T. N. Le, S. S. A. An, J. W. Han, M. I. Kim and J. Lee, *Adv. Funct. Mater.*, 2020, **30**, 1905410.

55 H. Shang, X. Zhou, J. Dong, A. Li, X. Zhao, Q. Liu, Y. Lin, J. Pei, Z. Li, Z. Jiang, D. Zhou, L. Zheng, Y. Wang, J. Zhou, Z. Yang, R. Cao, R. Sarangi, T. Sun, X. Yang, X. Zheng,

This journal is © The Royal Society of Chemistry 2022

J. Mater. Chem. A, 2022, **10**, 5717–5742 | **5737**

W. Yan, Z. Zhuang, J. Li, W. Chen, D. Wang, J. Zhang and Y. Li, *Nat. Commun.*, 2020, **11**, 3049.

56 C. Ma, B. Liu and S. Yan, *Mol. Catal.*, 2020, **495**, 111165.

57 Y. Chen, H. Li, W. Zhao, W. Zhang, J. Li, W. Li, X. Zheng, W. Yan, W. Zhang, J. Zhu, R. Si and J. Zeng, *Nat. Commun.*, 2019, **10**, 1885.

58 S. Wei, Y. Wang, W. Chen, Z. Li, W. C. Cheong, Q. Zhang, Y. Gong, L. Gu, C. Chen, D. Wang, Q. Peng and Y. Li, *Chem. Sci.*, 2020, **11**, 786–790.

59 Y. Wang, J. Mao, X. Meng, L. Yu, D. Deng and X. Bao, *Chem. Rev.*, 2019, **119**, 1806–1854.

60 A. Alarawi, V. Ramalingam and J.-H. He, *Mater. Today Energy*, 2019, **11**, 1–23.

61 J. Zhang, Y. Zhao, X. Guo, C. Chen, C.-L. Dong, R.-S. Liu, C.-P. Han, Y. Li, Y. Gogotsi and G. Wang, *Nat. Catal.*, 2018, **1**, 985–992.

62 V. Ramalingam, P. Varadhan, H. C. Fu, H. Kim, D. Zhang, S. Chen, L. Song, D. Ma, Y. Wang, H. N. Alshareef and J. H. He, *Adv. Mater.*, 2019, **31**, 1903841.

63 H. Su, L. Chen, Y. Chen, R. Si, Y. Wu, X. Wu, Z. Geng, W. Zhang and J. Zeng, *Angew. Chem., Int. Ed.*, 2020, **59**, 20411–20416.

64 L. Lin, Q. Yu, M. Peng, A. Li, S. Yao, S. Tian, X. Liu, A. Li, Z. Jiang, R. Gao, X. Han, Y.-W. Li, X.-D. Wen, W. Zhou and D. Ma, *J. Am. Chem. Soc.*, 2021, **143**, 309–317.

65 X. Zhang, M. Zhang, Y. Deng, M. Xu, L. Artiglia, W. Wen, R. Gao, B. Chen, S. Yao, X. Zhang, M. Peng, J. Yan, A. Li, Z. Jiang, X. Gao, S. Cao, C. Yang, A. J. Kropf, J. Shi, J. Xie, M. Bi, J. A. van Bokhoven, Y.-W. Li, X. Wen, M. Flytzani-Stephanopoulos, C. Shi, W. Zhou and D. Ma, *Nature*, 2021, **589**, 396–401.

66 S. Hoang, Y. Guo, A. J. Binder, W. Tang, S. Wang, J. Liu, T. D. Huan, X. Lu, Y. Wang, Y. Ding, E. A. Kyriakidou, J. Yang, T. J. Toops, T. J. Pauly, R. Ramprasad and P.-X. Gao, *Nat. Commun.*, 2020, **11**, 1062.

67 D. Kunwar, S. Zhou, A. DeLaRiva, E. J. Peterson, H. Xiong, X. I. Pereira-Hernandez, S. C. Purdy, R. ter Veen, H. H. Brongersma, J. T. Miller, H. Hashiguchi, L. Kovarik, S. Lin, H. Guo, Y. Wang and A. K. Datye, *ACS Catal.*, 2019, **9**, 3978–3990.

68 P. Xie, T. Pu, A. Nie, S. Hwang, S. C. Purdy, W. Yu, D. Su, J. T. Miller and C. Wang, *ACS Catal.*, 2018, **8**, 4044–4048.

69 Y. Wang, Z. Chen, P. Han, Y. Du, Z. Gu, X. Xu and G. Zheng, *ACS Catal.*, 2018, **8**, 7113–7119.

70 A. S. Hoffman, L. M. Debefve, S. Zhang, J. E. Perez-Aguilar, E. T. Conley, K. R. Justl, I. Arslan, D. A. Dixon and B. C. Gatesr, *ACS Catal.*, 2018, **8**, 3489–3498.

71 F. Dvorak, M. F. Camellone, A. Tovt, T. Nguyen-Dung, F. R. Negreiros, M. Vorokhta, T. Skala, I. Matolinova, J. Myslivecek, V. Matolin and S. Fabris, *Nat. Commun.*, 2016, **7**, 10801.

72 B. Qiao, J. Liu, Y.-G. Wang, Q. Lin, X. Liu, A. Wang, J. Li, T. Zhang and J. Liu, *ACS Catal.*, 2015, **5**, 6249–6254.

73 Z. L. Zhang, Y. H. Zhu, H. Asakura, B. Zhang, J. G. Zhang, M. X. Zhou, Y. Han, T. Tanaka, A. Q. Wang, T. Zhang and N. Yan, *Nat. Commun.*, 2017, **8**, 16100.

74 F. Wang, J. Ma, S. Xin, Q. Wang, J. Xu, C. Zhang, H. He and X. C. Zeng, *Nat. Commun.*, 2020, **11**, 529.

75 R. Qin, L. Zhou, P. Liu, Y. Gong, K. Liu, C. Xu, Y. Zhao, L. Gu, G. Fu and N. Zheng, *Nat. Catal.*, 2020, **3**, 703–709.

76 L. Kuai, Z. Chen, S. Liu, E. Kan, N. Yu, Y. Ren, C. Fang, X. Li, Y. Li and B. Geng, *Nat. Commun.*, 2020, **11**, 48.

77 K. Yang, Y. Liu, J. Deng, X. Zhao, J. Yang, Z. Han, Z. Hou and H. Dai, *Appl. Catal., B*, 2019, **244**, 650–659.

78 A. Parastaev, V. Muravev, E. H. Osta, A. J. F. van Hoof, T. F. Kimpel, N. Kosinov and E. J. M. Hensen, *Nat. Catal.*, 2020, **3**, 526–533.

79 T. W. van Deelen, C. H. Mejia and K. P. de Jong, *Nat. Catal.*, 2019, **2**, 955–970.

80 B. Han, Y. Guo, Y. Huang, W. Xi, J. Xu, J. Luo, H. Qi, Y. Ren, X. Liu, B. Qiao and T. Zhang, *Angew. Chem., Int. Ed.*, 2020, **59**, 11824–11829.

81 G. S. Parkinson, *Surf. Sci. Rep.*, 2016, **71**, 272–365.

82 J.-X. Liang, J. Lin, J. Liu, X. Wang, T. Zhang and J. Li, *Angew. Chem., Int. Ed.*, 2020, **59**, 12868–12875.

83 J. Liang, Q. Yu, X. Yang, T. Zhang and J. Li, *Nano Res.*, 2018, **11**, 1599–1611.

84 J. Lin, Y. Chen, Y. Zhou, L. Li, B. Qiao, A. Wang, J. Liu, X. Wang and T. Zhang, *AIChE J.*, 2017, **63**, 4003–4012.

85 J.-X. Liang, X.-F. Yang, A. Wang, T. Zhang and J. Li, *Catal. Sci. Technol.*, 2016, **6**, 6886–6892.

86 Q. Li, Z. Li, Q. Zhang, L. Zheng, W. Yan, X. Liang, L. Gu, C. Chen, D. Wang, Q. Peng and Y. Li, *Nano Res.*, 2020, **14**, 1435–1442.

87 J.-X. Liang, J. Lin, X.-F. Yang, A.-Q. Wang, B.-T. Qiao, J. Liu, T. Zhang and J. Li, *J. Phys. Chem. C*, 2014, **118**, 21945–21951.

88 J. Lin, A. Wang, B. Qiao, X. Liu, X. Yang, X. Wang, J. Liang, J. Li, J. Liu and T. Zhang, *J. Am. Chem. Soc.*, 2013, **135**, 15314–15317.

89 M. D. Marcinkowski, S. F. Yuk, N. Doudin, R. S. Smith, N. Manh-Thuong, B. D. Kay, V.-A. Glezakou, R. Rousseau and Z. Dohnalek, *ACS Catal.*, 2019, **9**, 10977–10982.

90 R. Bliem, J. Pavelec, O. Gamba, E. McDermott, Z. Wang, S. Gerhold, M. Wagner, J. Osiecki, K. Schulte, M. Schmid, P. Blaha, U. Diebold and G. S. Parkinson, *Phys. Rev. B: Condens. Matter Mater. Phys.*, 2015, **92**, 075440.

91 Z. Novotny, G. Argentero, Z. Wang, M. Schmid, U. Diebold and G. S. Parkinson, *Phys. Rev. Lett.*, 2012, **108**, 216103.

92 W. Qu, X. Liu, J. Chen, Y. Dong, X. Tang and Y. Chen, *Nat. Commun.*, 2020, **11**, 1532.

93 R. Lang, W. Xi, J.-C. Liu, Y.-T. Cui, T. Li, A. F. Lee, F. Chen, Y. Chen, L. Li, L. Li, J. Lin, S. Miao, X. Liu, A.-Q. Wang, X. Wang, J. Luo, B. Qiao, J. Li and T. Zhang, *Nat. Commun.*, 2019, **10**, 234.

94 J. Paier, C. Penschke and J. Sauer, *Chem. Rev.*, 2013, **113**, 3949–3985.

95 L. Nie, D. Mei, H. Xiong, B. Peng, Z. Ren, X. I. P. Hernandez, A. DeLariva, M. Wang, M. H. Engelhard, L. Kovarik, A. K. Datye and Y. Wang, *Science*, 2017, **358**, 1419–1423.

96 A. Jan, J. Shin, J. Ahn, S. Yang, K. J. Yoon, J.-W. Son, H. Kim, J.-H. Lee and H.-I. Ji, *RSC Adv.*, 2019, **9**, 27002–27012.

97 C. Riley, S. Zhou, D. Kunwar, A. De La Riva, E. Peterson, R. Payne, L. Gao, S. Lin, H. Guo and A. Datye, *J. Am. Chem. Soc.*, 2018, **140**, 12964–12973.

98 Y. Pang, W. Zang, Z. Kou, L. Zhang, G. Xu, J. Lv, X. Gao, Z. Pan, J. Wang and Y. Wu, *Nanoscale*, 2020, **12**, 4302–4308.

99 H. Wei, K. Huang, D. Wang, R. Zhang, B. Ge, J. Ma, B. Wen, S. Zhang, Q. Li, M. Lei, C. Zhang, J. Irawan, L.-M. Liu and H. Wu, *Nat. Commun.*, 2017, **8**, 1490.

100 K. P. Kuhn, I. F. Chaberny, K. Massholder, M. Stickler, V. W. Benz, H. G. Sonntag and L. Erdinger, *Chemosphere*, 2003, **53**, 71–77.

101 A. J. Therrien, A. J. R. Hensley, M. D. Marcinkowski, R. Zhang, F. R. Lucci, B. Coughlin, A. C. Schilling, J.-S. McEwen and E. C. H. Sykes, *Nat. Catal.*, 2018, **1**, 192–198.

102 H. Zhou, X. Yang, A. Wang, S. Miao, X. Liu, X. Pan, Y. Su, L. Li, Y. Tan and T. Zhang, *Chin. J. Catal.*, 2016, **37**, 692–699.

103 X. Zhou, Q. Shen, K. Yuan, W. Yang, Q. Chen, Z. Geng, J. Zhang, X. Shao, W. Chen, G. Xu, X. Yang and K. Wu, *J. Am. Chem. Soc.*, 2018, **140**, 554–557.

104 G. Busca, *Catal. Today*, 2014, **226**, 2–13.

105 J. M. Clary, S. A. Van Norman, H. H. Funke, D. Su, C. B. Musgrave and A. W. Weimer, *Nanotechnology*, 2020, **31**, 175703.

106 H. Shang, W. Chen, Z. Jiang, D. Zhou and J. Zhang, *Chem. Commun.*, 2020, **56**, 3127–3130.

107 Y. Lu, J. Wang, L. Yu, L. Kovarik, X. Zhang, A. S. Hoffman, A. Gallo, S. R. Bare, D. Sokaras, T. Kroll, V. Dagle, H. Xin and A. M. Karim, *Nat. Catal.*, 2019, **2**, 149–156.

108 F. Yan, C. Zhao, L. Yi, J. Zhang, B. Ge, T. Zhang and W. Li, *Chin. J. Catal.*, 2017, **38**, 1613–1620.

109 Y. Jing, Z. Cai, C. Liu, T. Toyao, Z. Maeno, H. Asakura, S. Hiwasa, S. Nagaoka, H. Kondoh and K.-i. Shimizu, *ACS Catal.*, 2020, **10**, 1010–1023.

110 H. Wang, J. Dong, L. F. Allard, S. Lee, S. Oh, J. Wang, W. Li, M. Shen and M. Yang, *Appl. Catal., B*, 2019, **244**, 327–339.

111 C. Dong and D. Ma, *Sci. China: Chem.*, 2020, **63**, 1584–1585.

112 Y. Xiong, W. Sun, Y. Han, P. Xin, X. Zheng, W. Yan, J. Dong, J. Zhang, D. Wang and Y. Li, *Nano Res.*, 2021, **14**, 2418–2423.

113 Y. Xiong, W. Sun, P. Xin, W. Chen, X. Zheng, W. Yan, L. Zheng, J. Dong, J. Zhang, D. Wang and Y. Li, *Adv. Mater.*, 2020, **32**, 2000896.

114 X. He, Y. Deng, Y. Zhang, Q. He, D. Xiao, M. Peng, Y. Zhao, H. Zhang, R. Luo, T. Gan, H. Ji and D. Ma, *Cell Rep. Phys. Sci.*, 2020, **1**, 100004.

115 J. Wang, Z. Li, Y. Wu and Y. Li, *Adv. Mater.*, 2018, **30**, 1801649.

116 L. H. Vieira, J. M. Assaf and E. M. Assaf, *Mater. Lett.*, 2020, **277**, 128354.

117 Y. Chen, S. Ji, W. Sun, W. Chen, J. Dong, J. Wen, J. Zhang, Z. Li, L. Zheng, C. Chen, Q. Peng, D. Wang and Y. Li, *J. Am. Chem. Soc.*, 2018, **140**, 7407–7410.

118 X.-L. Wang, X.-P. Fu, W.-W. Wang, C. Ma, R. Si and C.-J. Jia, *J. Phys. Chem. C*, 2019, **123**, 9001–9012.

119 X. I. Percira-Hcrnandcz, A. DeLaRiva, V. Muravev, D. Kunwar, H. Xiong, B. Sudduth, M. Engelhard, L. Kovarlk, E. J. M. Hcnscn, Y. Wang and A. K. Datye, *Nat. Commun.*, 2019, **10**, 1358.

120 M. J. Islam, M. G. Mesa, A. Osatiashtiani, M. J. Taylor, J. C. Manayil, C. M. A. Parlett, M. A. Isaacs and G. Kyriakou, *Appl. Catal., B*, 2020, **273**, 119062.

121 S. Tian, W. Gong, W. Chen, N. Lin, Y. Zhu, Q. Feng, Q. Xu, Q. Fu, C. Chen, J. Luo, W. Yan, H. Zhao, D. Wang and Y. Li, *ACS Catal.*, 2019, **9**, 5223–5230.

122 K. Mou, Z. Chen, X. Zhang, M. Jiao, X. Zhang, X. Ge, W. Zhang and L. Liu, *Small*, 2019, **15**, 1903668.

123 D. Ji, L. Fan, L. Li, S. Peng, D. Yu, J. Song, S. Ramakrishna and S. Guo, *Adv. Mater.*, 2019, **31**, 1808267.

124 J. Wan, W. Chen, C. Jia, L. Zheng, J. Dong, X. Zheng, Y. Wang, W. Yan, C. Chen, Q. Peng, D. Wang and Y. Li, *Adv. Mater.*, 2018, **30**, 1808267.

125 J. Kim, C.-W. Roh, S. K. Sahoo, S. Yang, J. Bae, J. W. Han and H. Lee, *Adv. Energy Mater.*, 2018, **8**, 1701476.

126 X. Shi, X. Wang, X. Shang, X. Zou, W. Ding and X. Lu, *ChemCatChem*, 2017, **9**, 3743–3751.

127 J. Chen, Y. Wanyan, J. Zeng, H. Fang, Z. Li, Y. Dong, R. Qin, C. Wu, D. Liu, M. Wang, Q. Kuang, Z. Xie and L. Zheng, *ACS Sustainable Chem. Eng.*, 2018, **6**, 14054–14062.

128 J. Zhang, X. Wu, W.-C. Cheong, W. Chen, R. Lin, J. Li, L. Zheng, W. Yan, L. Gu, C. Chen, Q. Peng, D. Wang and Y. Li, *Nat. Commun.*, 2018, **9**, 1002.

129 H. Wang, J. Shen, J. Huang, T. Xu, J. Zhu, Y. Zhu and C. Li, *Nanoscale*, 2017, **9**, 16817–16825.

130 X. Wang, X.-P. Fu, W.-Z. Yu, C. Ma, C.-J. Jia and R. Si, *Inorg. Chem. Front.*, 2017, **4**, 2059–2067.

131 Z. Bo, L. R. McCullough, S. Dull, M. A. Ardagh, J. Wang and J. Notestein, *J. Chem. Phys.*, 2019, **151**, 214703.

132 L. DeRita, S. Dai, K. Lopez-Zepeda, N. Pham, G. W. Graham, X. Pan and P. Christopher, *J. Am. Chem. Soc.*, 2017, **139**, 14150–14165.

133 M. Kottwitz, Y. Li, R. M. Palomino, Z. Liu, G. Wang, Q. Wu, J. Huang, J. Timoshenko, S. D. Senanayake, M. Balasubramanian, D. Lu, R. G. Nuzzo and A. I. Frenkel, *ACS Catal.*, 2019, **9**, 8738–8748.

134 J. Lu, J. W. Elam and P. C. Stair, *Surf. Sci. Rep.*, 2016, **71**, 410–472.

135 H. Wang and J. Lu, *Acta Phys.-Chim. Sin.*, 2018, **34**, 1334–1357.

136 J. Lu, J. W. Elam and P. C. Stair, *Acc. Chem. Res.*, 2013, **46**, 1806–1815.

137 P. Z. Chen, T. P. Zhou, L. L. Xing, K. Xu, Y. Tong, H. Xie, L. D. Zhang, W. S. Yan, W. S. Chu, C. Z. Wu and Y. Xie, *Angew. Chem., Int. Ed.*, 2017, **56**, 610–614.

138 B. Y. Xia, H. B. Wu, N. Li, Y. Yan, X. W. Lou and X. Wang, *Angew. Chem., Int. Ed.*, 2015, **54**, 3797–3801.

139 S. Sun, G. Zhang, N. Gauquelin, N. Chen, J. Zhou, S. Yang, W. Chen, X. Meng, D. Geng, M. N. Banis, R. Li, S. Ye, S. Knights, G. A. Botton, T.-K. Sham and X. Sun, *Sci. Rep.*, 2013, **3**, 1775.

140 H. Shang, W. Sun, R. Sui, J. Pei, L. Zheng, J. Dong, Z. Jiang, D. Zhou, Z. Zhuang, W. Chen, J. Zhang, D. Wang and Y. Li, *Nano Lett.*, 2020, **20**, 5443–5450.

This journal is © The Royal Society of Chemistry 2022

J. Mater. Chem. A, 2022, **10**, 5717–5742 | **5739**

141 C. Wang, H. Tissot, J. H. Stenlid, S. Kaya and J. Weissenrieder, *J. Phys. Chem. Lett.*, 2019, **10**, 7318–7323.

142 U. Heiz, A. Sanchez, S. Abbet and W. D. Schneider, *J. Am. Chem. Soc.*, 1999, **121**, 3214–3217.

143 S. Abbet, A. Sanchez, U. Heiz, W. D. Schneider, A. M. Ferrari, G. Pacchioni and N. Rosch, *J. Am. Chem. Soc.*, 2000, **122**, 3453–3457.

144 S. Proch, M. Wirth, H. S. White and S. L. Anderson, *J. Am. Chem. Soc.*, 2013, **135**, 3073–3086.

145 J. Liu, B. R. Bunes, L. Zang and C. Wang, *Environ. Chem. Lett.*, 2018, **16**, 477–505.

146 S. Wei, A. Li, J.-C. Liu, Z. Li, W. Chen, Y. Gong, Q. Zhang, W.-C. Cheong, Y. Wang, L. Zheng, H. Xiao, C. Chen, D. Wang, Q. Peng, L. Gu, X. Han, J. Li and Y. Li, *Nat. Nanotechnol.*, 2018, **13**, 856–861.

147 Z. Huang, X. Gu, Q. Cao, P. Hu, J. Hao, J. Li and X. Tang, *Angew. Chem., Int. Ed.*, 2012, **51**, 4198–4203.

148 J. Yu, A. Wang, W. Yu, X. Liu, X. Li, H. Liu, Y. Hu, Y. Wu and W. Zhou, *Appl. Catal., B*, 2020, **277**, 119236.

149 K. Liu, X. Zhao, G. Ren, T. Yang, Y. Ren, A. F. Lee, Y. Su, X. Pan, J. Zhang, Z. Chen, J. Yang, X. Liu, T. Zhou, W. Xi, J. Luo, C. Zeng, H. Matsumoto, W. Liu, Q. Jiang, K. Wilson, A. Wang, B. Qiao, W. Li and T. Zhang, *Nat. Commun.*, 2020, **11**, 1263.

150 A. Han, J. Zhang, W. Sun, W. Chen, S. Zhang, Y. Han, Q. Feng, L. Zheng, L. Gu, C. Chen, Q. Peng, D. Wang and Y. Li, *Nat. Commun.*, 2019, **10**, 3787.

151 M. Flytzani-Stephanopoulos, *Acc. Chem. Res.*, 2014, **47**, 783–792.

152 Q. Fu, W. L. Deng, H. Saltsburg and M. Flytzani-Stephanopoulos, *Appl. Catal., B*, 2005, **56**, 57–68.

153 L. Wang, W. Zhang, S. Wang, Z. Gao, Z. Luo, X. Wang, R. Zeng, A. Li, H. Li, M. Wang, X. Zheng, J. Zhu, W. Zhang, C. Ma, R. Si and J. Zeng, *Nat. Commun.*, 2016, **7**, 14036.

154 H. Xu, T. Liu, S. Bai, L. Li, Y. Zhu, J. Wang, S. Yang, Y. Li, Q. Shao and X. Huang, *Nano Lett.*, 2020, **20**, 5482–5489.

155 X. Ge, P. Zhou, Q. Zhang, Z. Xia, S. Chen, P. Gao, Z. Zhang, L. Gu and S. Guo, *Angew. Chem., Int. Ed.*, 2020, **59**, 232–236.

156 A. V. Crewe, J. Wall and J. Lanomore, *Science*, 1970, **168**, 1338–1340.

157 S. Duan, R. Wang and J. Liu, *Nanotechnology*, 2018, **29**, 204002.

158 J. Liu, *Chin. J. Catal.*, 2017, **38**, 1460–1472.

159 C. Wang, X.-K. Gu, H. Yan, Y. Lin, J. Li, D. Liu, W.-X. Li and J. Lu, *ACS Catal.*, 2017, **7**, 887–891.

160 S. B. Rice, J. Y. Koo, M. M. Disko and M. M. J. Treacy, *Ultramicroscopy*, 1990, **34**, 108–118.

161 T. Sun, Y. Li, T. Cui, L. Xu, Y. G. Wang, W. Chen, P. Zhang, T. Zheng, X. Fu, S. Zhang, Z. Zhang, D. Wang and Y. Li, *Nano Lett.*, 2020, **20**, 6206–6214.

162 H. Li, L. Wang, Y. Dai, Z. Pu, Z. Lao, Y. Chen, M. Wang, X. Zheng, J. Zhu, W. Zhang, R. Si, C. Ma and J. Zeng, *Nat. Nanotechnol.*, 2018, **13**, 411–417.

163 Z. Jiang, X. Feng, J. Deng, C. He, M. Douthwaite, Y. Yu, J. Liu, Z. Hao and Z. Zhao, *Adv. Funct. Mater.*, 2019, **29**, 1902041.

164 M. D. Marcinkowski, M. T. Darby, J. Liu, J. M. Wimble, F. R. Lucci, S. Lee, A. Michaelides, M. Flytzani-Stephanopoulos, M. Stamatakis and E. C. H. Sykes, *Nat. Chem.*, 2018, **10**, 325–332.

165 S. Koust, L. Arnarson, P. G. Moses, Z. Li, I. Beinik, J. V. Lauritsen and S. Wendt, *Phys. Chem. Chem. Phys.*, 2017, **19**, 9424–9431.

166 A. Mellor, D. Humphrey, C. M. Yim, C. L. Pang, H. Idriss and G. Thornton, *J. Phys. Chem. C*, 2017, **121**, 24721–24725.

167 C. Ye, N. Zhang, D. Wang and Y. Li, *Chem. Commun.*, 2020, **56**, 7687–7697.

168 B. C. Gates, *Chem. Rev.*, 1995, **95**, 511–522.

169 G. V. Korshin, A. I. Frenkel and E. A. Stern, *Environ. Sci. Technol.*, 1998, **32**, 2699–2705.

170 R. B. Greegor and F. W. Lytle, *J. Catal.*, 1980, **63**, 476–486.

171 F. de Groot, *Chem. Rev.*, 2001, **101**, 1779–1808.

172 H. Zhang, G. Liu, L. Shi and J. Ye, *Adv. Energy Mater.*, 2018, **8**, 1701343.

173 O. Alexeev and B. C. Gates, *Top. Catal.*, 2000, **10**, 273–293.

174 J. J. Rehr and R. C. Albers, *Rev. Mod. Phys.*, 2000, **72**, 621–654.

175 Q. Wang, X. Huang, Z. L. Zhao, M. Wang, B. Xiang, J. Li, Z. Feng, H. Xu and M. Gu, *J. Am. Chem. Soc.*, 2020, **142**, 7425–7433.

176 B. B. Sarma, P. N. Plessow, G. Agostini, P. Concepcion, N. Pfaender, L. Kang, F. R. Wang, F. Studt and G. Prieto, *J. Am. Chem. Soc.*, 2020, **142**, 14890–14902.

177 N. C. Nelson, L. Chen, D. Meira, L. Kovarik and J. Szanyi, *Angew. Chem., Int. Ed.*, 2020, **59**, 17657–17663.

178 L. Yuan, S.-F. Hung, Z.-R. Tang, H. M. Chen, Y. Xiong and Y.-J. Xu, *ACS Catal.*, 2019, **9**, 4824–4833.

179 L. Ye, X. Duan, S. Wu, T.-S. Wu, Y. Zhao, A. W. Robertson, H.-L. Chou, J. Zheng, T. Ayvali, S. Day, C. Tang, Y.-L. Soo, Y. Yuan and S. C. E. Tsang, *Nat. Commun.*, 2019, **10**, 914.

180 K. Siegbahn, C. Nordling, A. Fahlman, K. Hamrin, J. Hedman, R. Nordberg, C. Johansson, T. Bergmark, S.-E. Karlsson, I. Lindgren and B. Lindberg, *Nova Acta Regiae Soc. Sci. Ups. 20.1-282*, Almqvist and Wiksells, 1967.

181 R. W. Joyner, M. W. Roberts and K. Yates, *Surf. Sci.*, 1979, **87**, 501–509.

182 Q. Shang, N. Tang, H. Qi, S. Chen, G. Xu, C. Wu, X. Pan, X. Wang and Y. Cong, *Chin. J. Catal.*, 2020, **41**, 1812–1817.

183 Y. Yao, S. Hu, W. Chen, Z. Q. Huang, W. Wei, T. Yao, R. Liu, K. Zang, X. Wang, G. Wu, W. Yuan, T. Yuan, B. Zhu, W. Liu, Z. Li, D. He, Z. Xue, Y. Wang, X. Zheng, J. Dong, C. R. Chang, Y. Chen, X. Hong, J. Luo, S. Wei, W. X. Li, P. Strasser, Y. Wu and Y. Li, *Nat. Catal.*, 2019, **2**, 304–313.

184 G. Giannakakis, A. Trimpalis, J. Shan, Z. Qi, S. Cao, J. Liu, J. Ye, J. Biener and M. Flytzani-Stephanopoulos, *Top. Catal.*, 2018, **61**, 475–486.

185 G. X. Pei, X. Y. Liu, X. Yang, L. Zhang, A. Wang, L. Li, H. Wang, X. Wang and T. Zhang, *ACS Catal.*, 2017, **7**, 1491–1500.

186 J. Liu, J. Shan, F. R. Lucci, S. Cao, E. C. H. Sykes and M. Flytzani-Stephanopoulos, *Catal. Sci. Technol.*, 2017, **7**, 4276–4284.

5740 | *J. Mater. Chem. A*, 2022, **10**, 5717–5742

This journal is © The Royal Society of Chemistry 2022

187 L. Zhang, A. Wang, J. T. Miller, X. Liu, X. Yang, W. Wang, L. Li, Y. Huang, C.-Y. Mou and T. Zhang, *ACS Catal.*, 2014, **4**, 1546–1553.

188 F. Xing, J. Jeon, T. Toyao, K.-i. Shimizu and S. Furukawa, *Chem. Sci.*, 2019, **10**, 8292–8298.

189 C. Lamberti, A. Zecchina, E. Groppo and S. Bordiga, *Chem. Soc. Rev.*, 2010, **39**, 4951–5001.

190 J. Ryczkowski, *Catal. Today*, 2001, **68**, 263–381.

191 C. Asokan, L. DeRita and P. Christopher, *Chin. J. Catal.*, 2017, **38**, 1473–1480.

192 F. Yang, S. Ding, H. Song and N. Yan, *Sci. China Mater.*, 2020, **63**, 982–992.

193 M.-M. Millet, G. Algara-Siller, S. Wrabetz, A. Mazheika, F. Girgsdies, D. Teschner, F. Seitz, A. Tarasov, S. V. Leychenko, R. Schloegl and E. Frei, *J. Am. Chem. Soc.*, 2019, **141**, 2451–2461.

194 Y. Lu, C.-T. Kuo, L. Kovarik, A. S. Hoffman, A. Boubnov, D. M. Driscoll, J. R. Morris, S. R. Bare and A. M. Karim, *J. Catal.*, 2019, **378**, 121–130.

195 A. J. Foster and R. F. Lobo, *Chem. Soc. Rev.*, 2010, **39**, 4783–4793.

196 M. J. Huelsey, B. Zhang, Z. Ma, H. Asakura, D. A. Do, W. Chen, T. Tanaka, P. Zhang, Z. Wu and N. Yan, *Nat. Commun.*, 2019, **10**, 1330.

197 C. Schilling, M. Ziemba, C. Hess and M. Veronica Ganduglia-Pirovano, *J. Catal.*, 2020, **383**, 264–272.

198 D. B. Burueva, L. M. Kovtunova, V. I. Bukhtiyarov, K. V. Kovtunov and I. V. Koptyug, *Chem.–Eur. J.*, 2019, **25**, 1420–1431.

199 W. Zhang, S. Xu, X. Han and X. Bao, *Chem. Soc. Rev.*, 2012, **41**, 192–210.

200 A. Brueckner, *Chem. Soc. Rev.*, 2010, **39**, 4673–4684.

201 K. Dyrek and M. Che, *Chem. Rev.*, 1997, **97**, 305–331.

202 Q. Shen, C. Cao, R. Huang, L. Zhu, X. Zhou, Q. Zhang, L. Gu and W. Song, *Angew. Chem., Int. Ed.*, 2020, **59**, 1216–1219.

203 S. Hejazi, S. Mohajernia, B. Osuagwu, G. Zoppellaro, P. Andryskova, O. Tomanec, S. Kment, R. Zboril and P. Schmuki, *Adv. Mater.*, 2020, **32**, 1908505.

204 S. M. Heald, *J. Synchrotron Radiat.*, 2015, **22**, 436–445.

205 J. Zhang, C. Liu and B. Zhang, *Small Methods*, 2019, **3**, 1800481.

206 Z. Xu, Y. Zhang, L. Qin, Q. Meng, Z. Xue, L. Qiu, G. Zhang, X. Guo and Q. Li, *Small*, 2020, **16**, 2002071.

207 Y. Lou, Y. Cai, W. Hu, L. Wang, Q. Dai, W. Zhan, Y. Guo, P. Hu, X.-M. Cao, J. Liu and Y. Guo, *ACS Catal.*, 2020, **10**, 6094–6101.

208 B. Qiao, J.-X. Liang, A. Wang, C.-Q. Xu, J. Li, T. Zhang and J. J. Liu, *Nano Res.*, 2015, **8**, 2913–2924.

209 Z. Jakub, J. Hulva, P. T. P. Ryan, D. A. A. Duncan, D. J. J. Payne, R. Bliem, M. Ulreich, P. Hofegger, F. Kraushofer, M. Meier, M. Schmid, U. Diebold and G. S. S. Parkinson, *Nanoscale*, 2020, **12**, 5866–5875.

210 W. Chen, Y. Ma, F. Li, L. Pan, W. Gao, Q. Xiang, W. Shang, C. Song, P. Tao, H. Zhu, X. Pan, T. Deng and J. Wu, *Adv. Funct. Mater.*, 2019, **29**, 1904278.

211 Q. Fu, H. Saltsburg and M. Flytzani-Stephanopoulos, *Science*, 2003, **301**, 935–938.

212 S. Yao, X. Zhang, W. Zhou, R. Gao, W. Xu, Y. Ye, L. Lin, X. Wen, P. Liu, B. Chen, E. Crumlin, J. Guo, Z. Zuo, W. Li, J. Xie, L. Lu, C. J. Kiely, L. Gu, C. Shi, J. A. Rodriguez and D. Ma, *Science*, 2017, **357**, 389–393.

213 Y. Xiang, J. He, N. Sun, Y. Fan, L. Yang, C. Fang and L. Kuai, *Microporous Mesoporous Mater.*, 2020, **308**, 110507.

214 S. C. Ammal and A. Heyden, *ACS Catal.*, 2019, **9**, 7721–7740.

215 X. Sun, J. Lin, Y. Zhou, L. Li, Y. Su, X. Wang and T. Zhang, *AIChE J.*, 2017, **63**, 4022–4031.

216 H. Guan, J. Lin, B. Qiao, S. Miao, A.-Q. Wang, X. Wang and T. Zhang, *AIChE J.*, 2017, **63**, 2081–2088.

217 M. Yan, X. Ma, Y. Yang, X. Wang, W. C. Cheong, Z. Chen, X. Xu, Y. Huang, S. Wang, C. Lian and Y. Li, *Nano Lett.*, 2018, **18**, 6017–6021.

218 S. C. Ammal and A. Heyden, *ACS Catal.*, 2017, **7**, 301–309.

219 M. Xing, L. Guo and Z. Hao, *Int. J. Quantum Chem.*, 2018, **118**, e25767.

220 J. Shan, M. Li, L. F. Allard, S. Lee and M. Flytzani-Stephanopoulos, *Nature*, 2017, **551**, 605–608.

221 D. Bajec, A. Kostyniuk, A. Pohar and B. Likozar, *Chem. Eng. J.*, 2020, **396**, 125182.

222 S. Bai, F. Liu, B. Huang, F. Li, H. Lin, T. Wu, M. Sun, J. Wu, Q. Shao, Y. Xu and X. Huang, *Nat. Commun.*, 2020, **11**, 954.

223 K. Harrath, X. Yu, H. Xiao and J. Li, *ACS Catal.*, 2019, **9**, 8903–8909.

224 Y. Kwon, T. Y. Kim, G. Kwon, J. Yi and H. Lee, *J. Am. Chem. Soc.*, 2017, **139**, 17694–17699.

225 X. Guo, G. Fang, G. Li, H. Ma, H. Fan, L. Yu, C. Ma, X. Wu, D. Deng, M. Wei, D. Tan, R. Si, S. Zhang, J. Li, L. Sun, Z. Tang, X. Pan and X. Bao, *Science*, 2014, **344**, 616–619.

226 Y. Tang, Y. Wei, Z. Wang, S. Zhang, Y. Li, L. Nguyen, Y. Li, Y. Zhou, W. Shen, F. F. Tao and P. Hu, *J. Am. Chem. Soc.*, 2019, **141**, 7283–7293.

227 M. Akri, S. Zhao, X. Li, K. Zang, A. F. Lee, M. A. Isaacs, W. Xi, Y. Gangarajula, J. Luo, Y. Ren, Y.-T. Cui, L. Li, Y. Su, X. Pan, W. Wen, Y. Pan, K. Wilson, L. Li, B. Qiao, H. Ishii, Y.-F. Liao, A. Wang, X. Wang and T. Zhang, *Nat. Commun.*, 2019, **10**, 5181.

228 Z. Zuo, S. Liu, Z. Wang, C. Liu, W. Huang, J. Huang and P. Liu, *ACS Catal.*, 2018, **8**, 9821–9835.

229 W.-J. Jang, J.-O. Shim, H.-M. Kim, S.-Y. Yoo and H.-S. Roh, *Catal. Today*, 2019, **324**, 15–26.

230 D. Pakhare and J. Spivey, *Chem. Soc. Rev.*, 2014, **43**, 7813–7837.

231 S. Li, J. Yang, C. Song, Q. Zhu, D. Xiao and D. Ma, *Adv. Mater.*, 2019, **31**, 1901796.

232 X. Meng, X. Cui, N. P. Rajan, L. Yu, D. Deng and X. Bao, *Chem*, 2019, **5**, 2296–2325.

233 P. Schwach, X. Pan and X. Bao, *Chem. Rev.*, 2017, **117**, 8497–8520.

234 D. A. Bulushev and J. R. H. Ross, *Catal. Rev.: Sci. Eng.*, 2018, **60**, 566–593.

235 X. Ye, C. Yang, X. Pan, J. Ma, Y. Zhang, Y. Ren, X. Liu, L. Li and Y. Huang, *J. Am. Chem. Soc.*, 2020, **142**, 19001–19005.

236 C. Rivera-Carcamo, C. Scarfiello, A. B. Garcia, Y. Tison, H. Martinez, W. Baaziz, O. Ersen, C. Le Berre and P. Serp,

This journal is © The Royal Society of Chemistry 2022

J. Mater. Chem. A, 2022, **10**, 5717–5742 | 5741

Adv. Mater. Interfaces, 2020, 2001777, DOI: 10.1002/admi.202001777.

237 M. Xia, J. Ding, X. Du, R. Shang and Q. Zhong, *J. Alloys Compd.*, 2019, **777**, 406–414.

238 Y. Wang, H. Arandiyan, J. Scott, K.-F. Aguey-Zinsou and R. Amal, *ACS Appl. Energy Mater.*, 2018, **1**, 6781–6789.

239 Y. Guo, S. Mei, K. Yuan, D.-J. Wang, H.-C. Liu, C.-H. Yan and Y.-W. Zhang, *ACS Catal.*, 2018, **8**, 6203–6215.

240 F. J. Caparros, L. Soler, M. D. Rossell, I. Angurell, L. Piccolo, O. Rossell and J. Llorca, *ChemCatChem*, 2018, **10**, 2365–2369.

241 S. Ni, H. Zhang, Y. Zhao, X. Li, Y. Sun, J. Qian, Q. Xu, P. Gao, D. Wu, K. Kato, M. Yamauchi and Y. Sun, *Chem. Eng. J.*, 2019, **366**, 631–638.

242 W. K. Xiang, Y. H. Zhao, Z. Jiang, X. P. Li, H. Zhang, Y. Sun, Z. J. Ning, F. P. Du, P. Gao, J. Qian, K. Kato, M. Yamauchi and Y. H. Sun, *J. Mater. Chem. A*, 2018, **6**, 23366–23377.

243 Y. Pan, K. Sun, S. Liu, X. Cao, K. Wu, W. C. Cheong, Z. Chen, Y. Wang, Y. Li, Y. Liu, D. Wang, Q. Peng, C. Chen and Y. Li, *J. Am. Chem. Soc.*, 2018, **140**, 2610–2618.

244 Z. Hu, X. Li, S. Zhang, Q. Li, J. Fan, X. Qu and K. Lv, *Small*, 2020, **16**, 2004583.